*Article*

# Toxicity of TiO$_2$ Nanoparticles: Validation of Alternative Models

**Mélanie M. Leroux [1,†], Zahra Doumandji [1,†], Laetitia Chézeau [2], Laurent Gaté [2], Sara Nahle [1], Romain Hocquel [1], Vadim Zhernovkov [3], Sylvie Migot [1], Jafar Ghanbaja [1], Céline Bonnet [4], Raphaël Schneider [5] , Bertrand H. Rihn [1], Luc Ferrari [1] and Olivier Joubert [1,*]**

[1] Institut Jean Lamour, UMR CNRS 7198, Université de Lorraine, CNRS, IJL, F-54000 Nancy, France; melanie.lovera-leroux@univ-lorraine.fr (M.M.L.); doumandji.zahra@gmail.com (Z.D.); sara.nahle@univ-lorraine.fr (S.N.); romain.hocquel@univ-lorraine.fr (R.H.); syvlie.migot@univ-lorraine.Fr (S.M.); jafar.ghanbaja@univ-lorraine.fr (J.G.); bertrand.rihn@univ-lorraine.fr (B.H.R.); luc.ferrari@univ-lorraine.fr (L.F.)

[2] Institut National de Recherche et de Sécurité, rue du Morvan, 54519 Vandœuvre-les-Nancy, France; laetitia.chezeau@hotmail.fr (L.C.); laurent.gate@inrs.fr (L.G.)

[3] Systems Biology Ireland, University College Dublin, Dublin 4, Ireland; vadim.zhernovkov@ucd.ie

[4] Université de Lorraine, CHRU-Nancy, Genetic Department, F-54000 Nancy, France; c.bonnet@univ-lorraine.fr

[5] Laboratoire Réactions et Génie des Procédés, Université de Lorraine, CNRS, LRGP, F-54000 Nancy, France; raphael.schneider@univ-lorraine.FR

[*] Correspondence: olivier.joubert@univ-lorraine.fr; Tel.: +33-3-72-74-26-94

[†] These authors contributed equally to this work.

check for
updates

**Abstract:** There are many studies concerning titanium dioxide (TiO$_2$) nanoparticles (NP) toxicity. Nevertheless, there are few publications comparing *in vitro* and *in vivo* exposure, and even less comparing air–liquid interface exposure (ALI) with other *in vitro* and *in vivo* exposures. The identification and validation of common markers under different exposure conditions are relevant for the development of smart and quick nanotoxicity tests. In this work, cell viability was assessed *in vitro* by WST-1 and LDH assays after the exposure of NR8383 cells to TiO$_2$ NP sample. To evaluate *in vitro* gene expression profile, NR8383 cells were exposed to TiO$_2$ NP during 4 h at 3 cm$^2$ of TiO$_2$ NP/cm$^2$ of cells or 19 µg/mL, in two settings—submerged cultures and ALI. For the *in vivo* study, Fischer 344 rats were exposed by inhalation to a nanostructured aerosol at a concentration of 10 mg/m$^3$, 6 h/day, 5 days/week for 4 weeks. This was followed immediately by gene expression analysis. The results showed a low cytotoxic potential of TiO$_2$ NP on NR8383 cells. Despite the absence of toxicity at the doses studied, the different exposures to TiO$_2$ NP induce 18 common differentially expressed genes (DEG) which are involved in mitosis regulation, cell proliferation and apoptosis and inflammation transport of membrane proteins. Among these genes, we noticed the upregulation of *Ccl4*, *Osm*, *Ccl7* and *Bcl3* genes which could be suggested as early response biomarkers after exposure to TiO$_2$ NP. On the other hand, the comparison of the three models helped us to validate the alternative ones, namely submerged and ALI approaches.

**Keywords:** titanium dioxide; nanoparticles; transcriptomics; rat; macrophages; ALI; toxicogenomics

## 1. Introduction

Among the nanomaterials used in industries, titanium dioxide (TiO$_2$) nanoparticles (NP) are one of the most used. TiO$_2$ NP are mainly used as pigments for their brightness, high refractive index, opacity and antimicrobial properties. They are also useful in many cosmetics applications such as

in makeup, sunscreen, toothpastes and personal care products [1,2]. In the medical domain, $TiO_2$ NP are used as components for prosthetic implants (hip, knees, dental implants) or in intravenous injection [3–5]. $TiO_2$ NP are also found in other various applications like paint, glass, electronic and water treatment industries [6–10].

Due to these various industrial uses, $TiO_2$ represent 70% of the total production volume of pigments worldwide and it is in the top five NPs used in consumer products and approximately four million tons of $TiO_2$ are produced annually worldwide [4]. Their wide use must be challenged for the potential adverse health effects they can induce. Thus, it is urgent to assess the risk of different exposures to $TiO_2$ nanoparticles. Indeed, the interaction of nanoparticles with living organisms could result in biologic damages. Many studies on pulmonary toxicity of $TiO_2$ NPs have been published so far and *in vivo* and *in vitro* data indicate that the main toxicity mechanisms induced by $TiO_2$ NPs include pulmonary inflammation and oxidative stress, as well as genotoxicity [4,11–14]. However, discrepant results about the genotoxicity of these nanomaterials could be found in the literature. Also, different *in vivo* studies showed an increased significant inflammation after ingestion of $TiO_2$ NP [15,16].

Considering this bulk of studies about $TiO_2$ nanoparticles (NP) toxicity, there are few publications comparing *in vitro* and *in vivo* exposures—and even fewer comparing air–liquid interface exposure (ALI) with other *in vitro* and *in vivo* exposures [17–19]. Therefore, the aim of this study was to identify markers of exposure of the airways to $TiO_2$ NP, by comparing classical submerged *in vitro*, ALI and *in vivo* exposures.

NR8383 rat lung macrophages are relevant due to their immune functions and it is a validated model for nanotoxicological studies [20,21]. In the present work, we used this cell line with two types of exposure (submerged and ALI) compared to an *in vivo* rat exposure [22] to validate alternative models for nanotoxicological studies.

The present study succeeded in establishing a correlation of deregulated genes, which can be considered as biomarkers of exposure to $TiO_2$ NPs and their associated molecular pathways on three different *in vivo* and *in vitro* models.

Here, after analyzing transcriptomes of the different models following three type of exposures to $TiO_2$ NP, we identified common genes and biologic pathways. This validates alternative models, which are cost and time effective and ethically more acceptable.

## 2. Results

### 2.1. TiO₂ Nanoparticles Characterization

The morphology of $TiO_2$ NP was observed under a transmission electron microscope (TEM). The size of the NM105 nanoparticles was $21.5 \pm 7.2$ nm (Figure 1) which is in accordance with the characteristics given by the supplier (Table 1). X-ray diffraction analysis showed that the NM-105 NP samples were composed of about 18% rutile and 82% anatase. The secondary size obtained by DLS was around 170 nm, the zeta potential was $11.1 \pm 0.7$ mV and the specific surface area was 51 $m^2$/g (Table 1).

**Table 1.** $TiO_2$ NP characteristics.

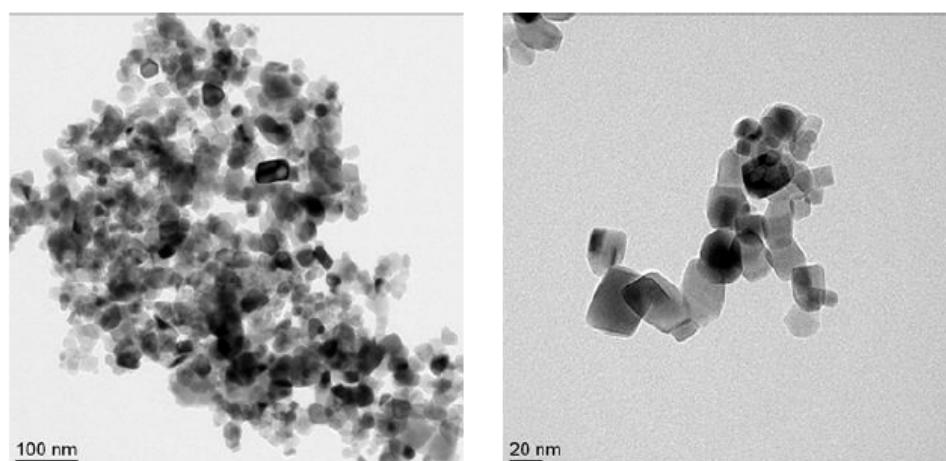| Nanoparticle | Primary Size (nm) | Secondary Size (nm) | Zeta Potential (mV) | Specific Surface Aera ($m^2$/g) | Provider |
|---|---|---|---|---|---|
| **TiO₂ (NM-105)** | $21.5 \pm 7.2$ | $170 \pm 1.5$ | $11.1 \pm 0.7$ | 51 | Joint Research Center |

**Figure 1.** TEM images of titanium dioxide nanoparticles. $TiO_2$ NPs (NM-105) in anatase dominant form.

## 2.2. In Vitro Cytotoxicity Study

Regardless of the tests and the doses (Figure 2), exposure of NR8383 cells to $TiO_2$ NP for 24 h did not statistically decrease their viability. Indeed, compared to cells not exposed to NM-105 NP, the metabolic activity measured by the WST-1 test was constant and the 10% decrease observed after a $TiO_2$ exposure of 100 µg/mL and 200 mg/mL was not statistically significant (Figure 2A). Nevertheless, the release of LDH into the extracellular medium increased up to 30 % in a statistically insignificant manner for 100-µg/mL and 200-mg/mL $TiO_2$ exposure (Figure 2B).
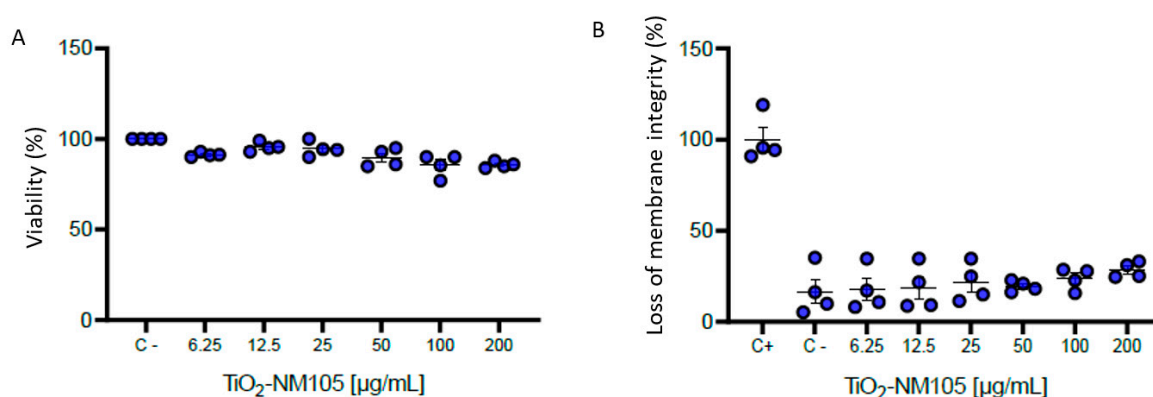


**Figure 2.** (**A**) Cytotoxicity of $TiO_2$ NP (24 h exposure) to NR8383 by WST-1 test and (**B**) loss of membrane integrity by LDH release measurement. Non exposed cells are negative control (C−) and positive control (C+) for LDH are cells exposed to the lysis buffer (Triton 5%) during 15 min before the measure. Data are presented as means ± standard deviation (SD) of the four biologic replicates.

## 2.3. Transcriptomic Analysis of Dysregulated Genes Following In Vivo, In Vitro Submerged, and ALI Vitrocell Cloud ® Exposure (ALI) to NM-105 $TiO_2$ NP

As represented by the volcano plot of dysregulated genes (Figure 3), ALI rat cells and lung exposed to $TiO_2$ NP by inhalation showed similar number of differentially expressed genes (DEGs), 851 and 1477, respectively, with a fold change > 1.3 (Table 2), while the number of genes dysregulated of *in vitro* submerged conditions with a fold change > 1.3 was ten times higher with 9836 DEGs (Table 2, Figure 3A). With a fold change > 3, we found 1721 genes differentially expressed genes in the *in vitro* submerged cells exposed to NM-105, but only 69 DEGs in *in vivo*. Interestingly, with a fold change of 3, a higher proportion of downregulated genes were found with *in vitro* submerged condition compared to *in vivo* exposure which showed more upregulated genes than downregulated (Table 2). Finally,

it is important to note that the transcriptomic study brings out only one DEG with a fold change > 3 in the case of ALI exposure, namely *Myc* (Figure 3C). Indeed, ALI exposure showed less DEGs genes with only 202 DEG with a fold change > 1.5 vs. 780 DEGs for *in vivo* exposure and 7895 for *in vitro* submerged exposure (Table 2).

**Table 2.** Total number of differentially expressed genes (FDR corrected *p*-value < 0.05).

| Groups | FC 1.3 | | | FC 1.5 | | | FC3 | | |
|---|---|---|---|---|---|---|---|---|---|
| | Up | Down | Total | Up | Down | Total | Up | Down | Total |
| *in vitro* submerged | 4612 | 5224 | **9836** | 3939 | 3956 | **7895** | 345 | 1376 | **1721** |
| *in vitro* ALI | 439 | 412 | **851** | 108 | 94 | **202** | 0 | 1 | **1** |
| lung | 898 | 579 | **1477** | 559 | 221 | **780** | 64 | 5 | **69** |



**Figure 3.** *Cont.*

**Figure 3.** Volcano plots displaying differentially expressed genes between NM-105 treated and control samples for (**A**) *in vitro* submerged, (**B**) *in vivo* lung and (**C**) *in vitro* ALI exposures. Vertical axis corresponds to the -$\log_{10}$(FDR corrected *p*-value) and the horizontal axis displays the log2-fold change value. The vertical lines correspond to 1.3-fold up and down changes ($\log_2$FC = 0.38), respectively, and the horizontal line represents FDR corrected *p*-value of 0.05 (-$\log_{10}$P = 1.3). Red dots represent the up- and downregulated expressed genes.

The gene spring analysis of the 20 most up-DEG and 20 down-DEG in the three conditions (Supplementary Data 1: Figure S1) allows to identify five KEGG pathways for *in vitro* submerged cells exposed to TiO$_2$ NP, including 'IL-17 signaling pathway', 'Chemokine signaling pathway' and 'Cytokine–cytokine receptor interaction': rno04657, rno0462, rno05323, rno04060, rno05144 (Figure S1A), emphasize the role of macrophages inflammation. No common pathway was identified in the analysis of *in vivo* and ALI DEGs. Interestingly, GO biologic process (BP) annotation showed 5 common biologic process between *in vivo* and ALI: 0080090, 0060255, 051172, 0051171, 0050896 (Figure S1B,C); all are involved in metabolic and cellular processes, while only one is common between *in vivo* and *in vitro* submerged condition, namely 0048545 (Figure S1A,B). No common BP for ALI and *in vitro* submerged conditions or for the three conditions were evidenced. More connections between the DEGs were found *in vitro* (22) and *in vivo* (16) than in ALI conditions (6), and for all the groups, the software indicated that the genes are at least partially biologically connected as a group (Figure S1).

### 2.4. Common Dysregulated Genes between In Vivo, In Vitro, and ALI Exposures to TiO$_2$ NP

Regarding the differences between the fold changes of *in vitro* submerged experiments, the results comparison was performed using a cutoff of 2.8 for *in vitro* submerged and 1.3 for both *in vivo* and *in vitro* ALI conditions with a *p*-value fixed to *p* < 0.05 for the three conditions. These cutoffs focus on the most deregulated genes in the three conditions and allow a better selective analysis for the comparison of the three exposures.

The Venn diagram of differentially dysregulated genes comparing TiO$_2$ NP exposition in the three conditions showed 18 common DEGs. 107 common DEGs were found between *in vivo* (lung) and *in vitro* submerged, 53 between *in vivo* (lung) and ALI exposures and 147 between *in vitro* submerged and ALI exposures (Figure 4).
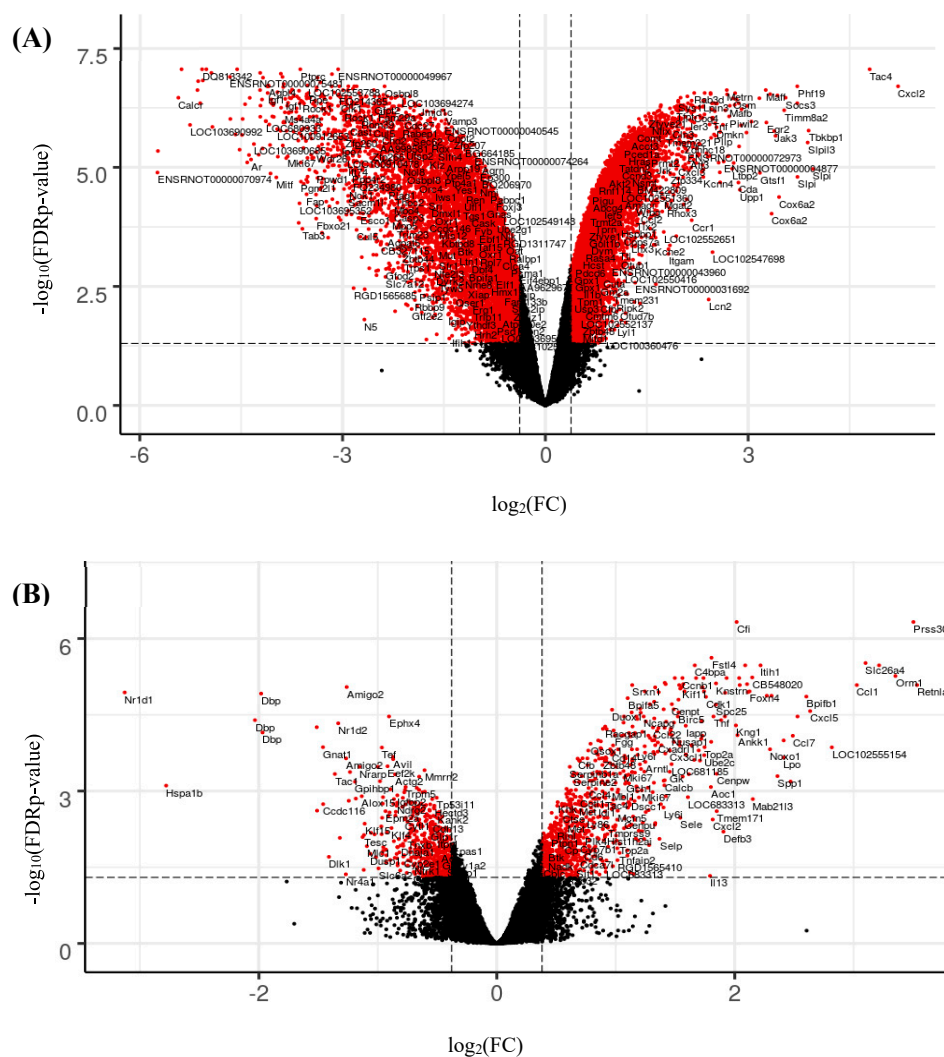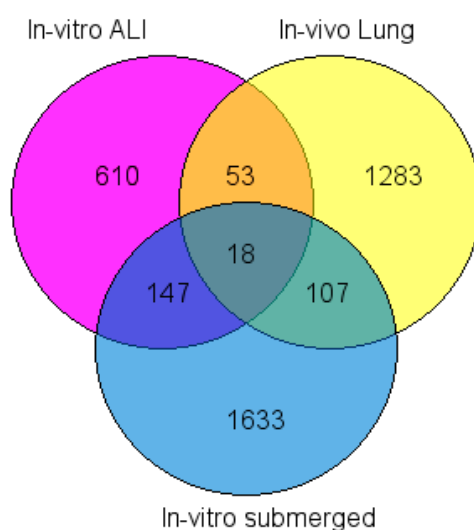
**Figure 4.** Venn diagram of differentially deregulated genes after TiO$_2$ NP *in vivo* (lung), *in vitro* submerged and ALI (Vitrocell) exposures (FDR corrected *p*-value < 0.05). Genes were filtered with different fold change cutoff: *In vitro* submerged: 2.8, *In vitro* ALI Vitrocell: 1.3 and *In vivo* lung: 1.3.

*2.5. Comparison of Functional Annotations of Dysregulated Genes In Vivo, In Vitro, and ALI after Exposition to TiO$_2$ NP*

GSEA analysis showed two common gene sets dysregulated in the three exposure, related to inflammation and oncogenesis: the IL6-JAK-STAT3 signaling and genes regulated by the transcription factor MYC (MYC_TARGETS_V2) (Table 3). Four common gene sets were found between *in vivo* and ALI exposure, among them genes implied in 'cell cycle regulation' (E2F_TARGETS, G2M_CHECKPOINT) and 'cell transformation' (EPITHELIAL_ MESENCHYMAL_TRANSITION). Interestingly, another group of genes regulated by the transcription factor MYC was found (MYC_TARGETS_V1), which can be clustered in a MYC_TARGETS group V1 and V2. Two common gene sets were found between *in vivo* and *in vitro* submerged exposures (UV_RESPONSE_DN and TNFA_SIGNALING_VIA_NFKB) and no common gene set was found between *in vitro* and in ALI conditions. Seventeen gene sets were found only in lung, which is not surprising because herein the cell types analyzed are heterogenous, notably composed of epithelial, immune and endothelial cells, whereas cultured cells are characterized by their homogeneity. These gene sets were related to inflammation, immune response and homeostasis. ALI exposure resulted in UV_RESPONSE_UP gene set which can be brought closer to those common between *in vivo* and *in vitro* submerged exposures, in a UV-RESPONSE dysregulation. Finally, three gene sets were found specifically for *in vitro* submerged samples (MITOTIC_SPINDLE, DNA_REPAIR and PROTEIN_SECRETION).

**Table 3.** Gene set enrichment analysis (GSEA) functional annotation of differentially expressed genes (DEG) in the three conditions.

| Gene Set | *p*-Value *in vivo* Lung | *p*-Value *in vitro* ALI | *p*-Value *in vitro* Submerged |
|---|---|---|---|
| **Common gene sets between the three exposures** | | | |
| IL6_JAK_STAT3_SIGNALING | $1.25 \times 10^{-7}$ | $7.42 \times 10^{-2}$ | $3.82 \times 10^{-2}$ |
| MYC_TARGETS_V2 | $4.30 \times 10^{-6}$ | $7.42 \times 10^{-2}$ | $3.65 \times 10^{-2}$ |
| **Common gene sets between *in vivo* and ALI exposures** | | | |
| E2F_TARGETS | $1.04 \times 10^{-14}$ | $8.40 \times 10^{-7}$ | – |
| G2M_CHECKPOINT | $7.96 \times 10^{-11}$ | $7.00 \times 10^{-3}$ | – |

**Table 3.** *Cont.*

| Gene Set | p-Value in vivo Lung | p-Value in vitro ALI | p-Value in vitro Submerged |
|---|---|---|---|
| MYC_TARGETS_V1 | $1.08 \times 10^{-4}$ | $7.00 \times 10^{-3}$ | – |
| EPITHELIAL_MESENCHYMAL_TRANSITION | $9.03 \times 10^{-2}$ | $3.84 \times 10^{-2}$ | – |
| **Common gene sets between *in vivo* and *in vitro* submerged exposures** | | | |
| UV_RESPONSE_DN | $6.21 \times 10^{-3}$ | – | $6.73 \times 10^{-2}$ |
| TNFA_SIGNALING_VIA_NFKB | $9.43 \times 10^{-3}$ | – | $1.46 \times 10^{-3}$ |
| **Non common gene sets** | | | |
| ALLOGRAFT_REJECTION | $1.25 \times 10^{-7}$ | – | – |
| MTORC1_SIGNALING | $5.73 \times 10^{-7}$ | – | – |
| INFLAMMATORY_RESPONSE | $1.48 \times 10^{-6}$ | – | – |
| MYOGENESIS | $4.30 \times 10^{-6}$ | – | – |
| INTERFERON_GAMMA_RESPONSE | $8.61 \times 10^{-4}$ | – | – |
| COMPLEMENT | $5.05 \times 10^{-3}$ | – | – |
| ANGIOGENESIS | $5.82 \times 10^{-3}$ | – | – |
| IL2_STAT5_SIGNALING | $2.32 \times 10^{-2}$ | – | – |
| CHOLESTEROL_HOMEOSTASIS | $3.89 \times 10^{-2}$ | – | – |
| APICAL_JUNCTION | $4.49 \times 10^{-2}$ | – | – |
| GLYCOLYSIS | $6.27 \times 10^{-2}$ | – | – |
| HEDGEHOG_SIGNALING | $6.27 \times 10^{-2}$ | – | – |
| WNT_BETA_CATENIN_SIGNALING | $8.13 \times 10^{-2}$ | – | – |
| COAGULATION | $8.89 \times 10^{-2}$ | – | – |
| TGF_BETA_SIGNALING | $9.03 \times 10^{-2}$ | – | – |
| OXIDATIVE_PHOSPHORYLATION | $9.03 \times 10^{-2}$ | – | – |
| UNFOLDED_PROTEIN_RESPONSE | $9.55 \times 10^{-2}$ | – | – |
| UV_RESPONSE_UP | – | $7.42 \times 10^{-2}$ | – |
| MITOTIC_SPINDLE | – | – | $9.38 \times 10^{-3}$ |
| DNA_REPAIR | – | – | $3.65 \times 10^{-2}$ |
| PROTEIN_SECRETION | – | – | $4.11 \times 10^{-2}$ |

*2.6. Functional Analysis of Common Dysregulated Genes between In Vivo, In Vitro, and ALI Expositions to TiO$_2$ NP*

Among the 18 common DEGs identified with the Venn diagram (Figure 4), four are upregulated in the three conditions: *Ccl4* (FC: 1.71; 3.72; 2.15 for *in vivo*, *in vitro* and ALI conditions, respectively), *Ccl7* (FC: 5.61; 3.53; 1.47) and *Osm* (FC: 1.38; 6.84; 1.41) which are involved in the same KEGG pathways (cytokine–cytokine receptor interaction) and *Bcl3* (FC: 1.69; 4.60; 1.41) which plays a role in cell proliferation (Tables 4 and 5B), while the others common DEGs displayed opposite up and down regulation. Indeed, 11 DEG are upregulated *in vivo* and downregulated *in vitro* and in ALI conditions. *Ppp2r5b* and *Osgin1* are upregulated *in vitro* and downregulated *in vivo* and *Ptpn13* is upregulated during *in vitro* submerged conditions and downregulated for both *in vivo* and ALI conditions (Figure 5). These differences can be explained easily by the experimental conditions as *in vivo* results are for the whole lung rat while *in vitro* and ALI conditions only for macrophages cell NR8383.
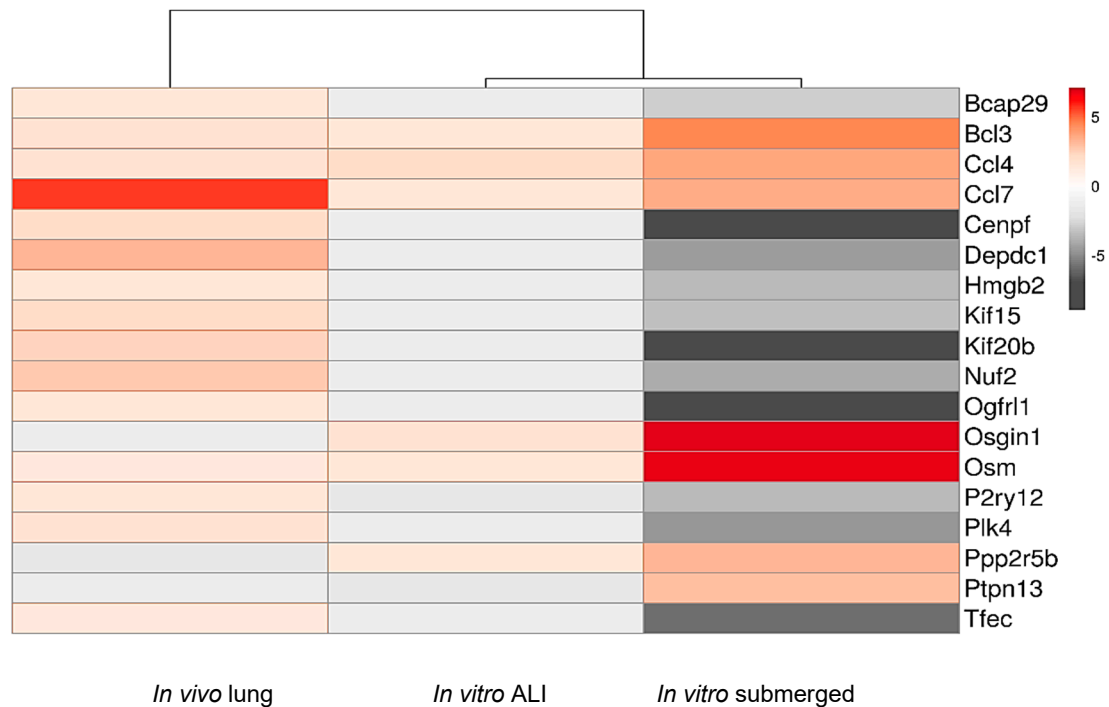
**Figure 5.** Heatmap of common dysregulated genes, fold changes are represented by a color scale (*p*-value < 0.05).

The 18 dysregulated genes common for the 3 exposure methods (Table 4, Figure 5) are involved in 'mitosis regulation', and evidenced by changes in (*i*) constitution of the kinetochore–centromere complex: *Cenpf*, *Nuf2*, *Nuf2*, *Kif15*, *Kif20b*, *Plk4*, (*ii*) mitosis regulation: *Depdc1* and (*iii*) chromatin remodeling: *Hmgb2*. Moreover significant changes were also evidenced in (*i*) 'cell proliferation and apoptosis' (*Bcl3*, *Osgin1*, *Ptpn13*, *Ppp2r5*, *Bcap29*), (*ii*) 'cell differentiation' (*Hmgb2*, *P2ry12*, *Tfec*, *Ogfrl1*, *Bcl3*, *Ptpn13*), (*iii*) 'inflammation' (*P2ry12*, *Ccl4*, *Ccl7*, *Osm*, *Tfec*, *Osgin1*) and (*iv*) a single gene related to transport of membrane proteins (*Bcap29*). KEGG pathway analysis found one common pathway for 3 genes (*Osm*, *Ccl4* and *Ccl7*), namely 'cytokine–cytokine receptor interaction pathway' that is involved in intracellular regulation and immune response, inflammation, cell growth, differentiation, cell death, angiogenesis, development and repair processes aimed at the restoration of homeostasis (Table 4, Figure 6). Unsurprisingly, several studies and databases showed that these 18 dysregulated genes are associated with tumorigenesis, cancer initiation progression and aggressiveness (Table 4).

GO-BP analysis of the 18 common DEGs between the three exposure methods highlight some groups functions: inflammation and immune response, cell migration, intracellular movements (Table 5A). Coherently, a KEGG analysis finds one pathway associated with inflammation: cytokine–cytokine receptor interaction pathway (RNO-04060) and Reactome analysis revealed five pathways implied in mitosis and transport: mitotic prometaphase (R-RNO-68877), separation of sister chromatids (RNO-2500257, RNO-2467813), kinetochore and actin functions (RNO-141444 and RNO-5663220) (Table 5B,C). When projected to human model, the same dysregulated pathways were found (Supplementary Figure S2, Table S2).

**Table 4.** Common genes between the three exposures (different group functions are highlighted in different colors, detailed information where found in GeneCards, UniProt, String, protein Atlas and PubMed databases). Colors in the function group column are used to identify common elements easily.

| Name Gene Protein | FC | | | Protein Function | Function Group *KEGG Pathway | Pathologies Associated |
|---|---|---|---|---|---|---|
| | Vivo | Vitro | ALI | | | |
| **Cenpf** **Centromere protein F** | 1.97 | −8.43 | −1.33 | The CENPF protein is a part of the corona of kinetochore complex which interacts with microtubules and participate to a precise and rapid chromosome segregation. [23] | **Mitosis** **kinetochore–centromere complex** | |
| **Nuf2** kinetochore protein Nuf2 | 2.66 | −4.05 | −1.31 | Component of the essential kinetochore-associated NDC80 complex, required for chromosome segregation and spindle checkpoint activity, required for kinetochore integrity. [24] | **Mitosis** **kinetochore–centromere complex** | |
| **Kif15** kinesin-like protein KIF15 | 2.11 | −3.35 | −1.38 | Plus-end directed kinesin-like motor enzyme involved in mitotic spindle assembly [25] | **Mitosis** **kinetochore–centromere complex** | |
| **Kif20b** kinesin family member 20B | 2.50 | −8.91 | −1.39 | Belongs to the TRAFAC class myosin–kinesin ATPase superfamily. kinesin family (String DB) | **Mitosis** **kinetochore–centromere complex** | |
| **Plk4** serine/threonine protein kinase | 1.67 | −4.64 | −1.36 | serine/threonine–protein kinase that plays a central role in centriole duplication; (UniProt) | **Mitosis** **kinetochore–centromere complex** | |
| **Depdc1** DEP domain containing 1 | 3.31 | −4.45 | −1.33 | DEP domain containing 1 (DEPDC1) is a highly conserved protein among many species. DEPDC1 was overexpressed in different types of cancers. [26] | **Mitosis regulation** [26] | **Cancer** [26] |
| **Hmgb2** high mobility group box 2 | 1.46 | −3.59 | −1.44 | Multifunctional protein with various roles in different cellular compartments. May act in a redox sensitive manner. In the nucleus is an abundant chromatin-associated non-histone protein involved in transcription, chromatin remodeling and V(D)J recombination. HMGBs act as architectural facilitators in the assembly of nucleoprotein complexes. [27] | **Mitosis** **chromatin remodeling** **T cells differentiation** | **Cancer** [28] [29] |
| **P2ry12** P2Y purinoceptor 12 | 1.43 | −3.54 | −1.58 | Receptor for ADP and ATP coupled to G-proteins. Required for normal platelet aggregation and blood coagulation. [30] | **Inflammation: chemotaxis receptor** **Cell differentiation** **Macrophages M1/M2** [31] | **Cancer** [31] |
| **Ccl4** C–C motif chemokine 4 | 1.71 | 3.72 | 2.15 | Monokine with inflammatory and chemokinetic properties; (UniProt) | **Inflammation: chemotaxis** *Cytokine–cytokine receptor interaction | **Inflammation diseases** |
| **Ccl7** C–C motif chemokine 7 | 5.61 | 3.53 | 1.47 | Chemotactic factor attracts monocytes and eosinophils, but not neutrophils. (String DB) | **Inflammation: chemotaxis** *Cytokine–cytokine receptor interaction | **Inflammation diseases** **Cancer** |
| **Osm** oncostatin-M | 1.38 | 6.84 | 1.41 | Growth regulator. It regulates cytokine production, including IL-6, G-CSF and GM-CSF; (UniProt) | **Inflammation: regulation** *Cytokine–cytokine receptor interaction | **Cancer** |
| **Tfec** transcription factor EC | 1.35 | −5.86 | −1.32 | transcriptional regulator that acts as a repressor or an activator; (UniProt) | **Cell differentiation** **Macrophages M2 activation** [32] **Inflammation** [33] | **Cancer** |
| **Ogfrl1** opioid growth factor receptor-like 1 | 1.47 | −7.00 | −1.32 | Mobilization and differentiation of bone marrow (BM)-derived cells [34] | **Cell differentiation** Upregulated in M2 macrophages [35] | **Cancer** [36] |
| **Bcl3** B-cell CLL/lymphoma 3 | 1.69 | 4.60 | 1.41 | BCL3 (BCL3 transcription Coactivator) is a proto-oncogene candidate. Its related pathways are Apoptosis-related network and Common cytokine receptor gamma-chain family signaling pathways. Contributes to the regulation of cell proliferation and to the regulation of transcriptional activation of NF-kappa-B target genes. (GeneCards) | **Cell proliferation** **Apoptosis regulation** | **Cancer** |

**Table 4.** *Cont.*

| Name Gene Protein | FC | | | Protein Function | Function Group *KEGG Pathway | Pathologies Associated |
|---|---|---|---|---|---|---|
| | **Vivo** | **Vitro** | **ALI** | | | |
| **Osgin1** oxidative stress induced growth inhibitor 1 | −1.38 | 7.10 | 1.74 | This gene encodes an oxidative stress response protein that regulates cell death. Expression regulated by p53 and induced by DNA damage. The protein regulates apoptosis by inducing cytochrome c release from mitochondria. Key regulator of both inflammatory and anti-inflammatory molecules. The loss of this protein correlates with uncontrolled cell growth and tumor formation. (GeneCards) | **Inflammation regulation** **Apoptosis regulation** | **Cancer** |
| **Ptpn13** protein tyrosine phosphatase non-receptor type 13 | −1.41 | 3.01 | −1.57 | Member of the protein tyrosine phosphatase (PTP) family. PTPs are signaling molecules that regulate a variety of cellular processes including cell growth, differentiation, mitotic cycle and oncogenic transformation. Regulates negatively FAS-induced apoptosis and NGFR-mediated pro-apoptotic signaling. (GeneCards) | **Cell proliferation and differentiation** **Apoptosis regulation** **Mitosis** Oncogenic transformation | **Amyloidosis Cancer** |
| **Ppp2r5b** serine/threonine protein phosphatase regulatory subunit beta isoform | −1.57 | 3.32 | 1.48 | The product of this gene belongs to the phosphatase 2A (PP2A) regulatory subunit B family. PP2A it is implicated in the negative control of cell growth and division. The phosphorylated form mediates the interaction between PP2A and AKT1. (GeneCards) | **Cell proliferation** | **Cancer** |
| **Bcap29** B-cell receptor-associated protein 29 | 1.54 | −2.90 | −1.38 | Among its related pathways are B Cell Receptor Signaling Pathway and AKT Signaling Pathway. May play a role in transport of membrane proteins. May be involved in CASP8-mediated apoptosis. (GeneCards) | **Transport of membrane protein** **Apoptosis** | |
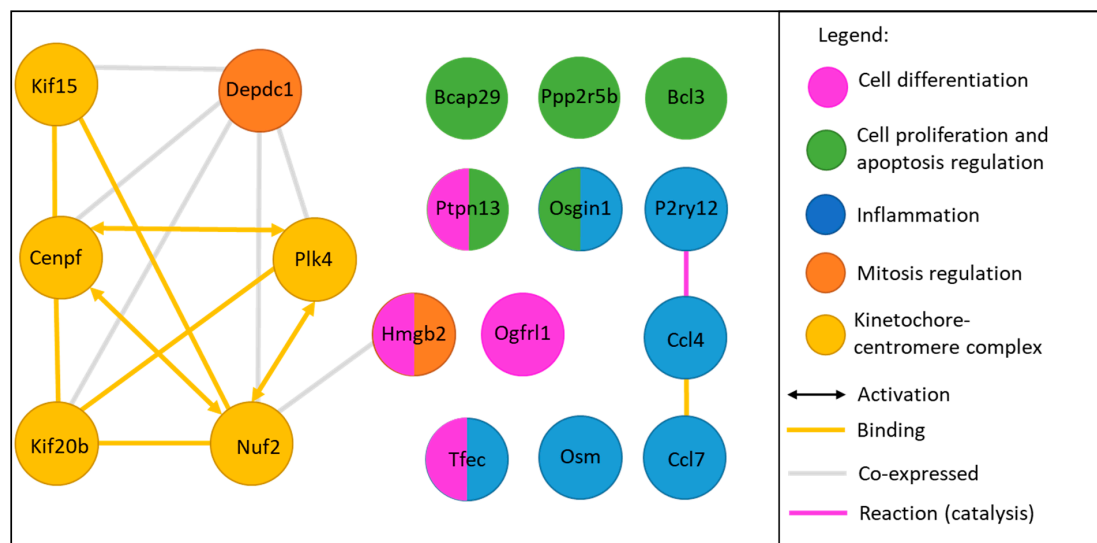


**Figure 6.** Interactions and function groups of the 18 common dysregulated genes (adapted from an analyze by String 11.1 Database, functions groups were determined through UniProt, GeneCards and PubMed researches).

**Table 5.** (**A**) Gene ontology (GO) biologic process (20 most dysregulated GO-term); (**B**) KEGG pathways and (**C**) reactome pathways of the 18 common dysregulated genes (analyzed by String 11.1 Database).

| (A) GO-term | Description | Count in Gene Set | False Discovery Rate |
|---|---|---|---|
| GO:0071346 | cellular response to interferon-gamma | 2 of 39 | 0.0265 |
| GO:0070098 | chemokine-mediated signaling pathway | 2 of 30 | 0.0265 |
| GO:0050921 | positive regulation of chemotaxis | 2 of 68 | 0.0265 |
| GO:0048522 | positive regulation of cellular process | 7 of 2201 | 0.0265 |
| GO:0048247 | lymphocyte chemotaxis | 2 of 20 | 0.0265 |
| GO:0045087 | innate immune response | 3 of 217 | 0.0265 |
| GO:0044089 | positive regulation of cellular component biogenesis | 3 of 220 | 0.0265 |
| GO:0040011 | locomotion | 4 of 404 | 0.0265 |
| GO:0030593 | neutrophil chemotaxis | 2 of 23 | 0.0265 |
| GO:0016477 | cell migration | 3 of 293 | 0.0265 |
| GO:0010469 | regulation of signaling receptor activity | 4 of 325 | 0.0265 |
| GO:0009967 | positive regulation of signal transduction | 4 of 638 | 0.0265 |
| GO:0006955 | immune response | 4 of 386 | 0.0265 |
| GO:0006954 | inflammatory response | 3 of 250 | 0.0265 |
| GO:0006935 | chemotaxis | 3 of 172 | 0.0265 |
| GO:0006928 | movement of cell or subcellular component | 4 of 486 | 0.0265 |
| GO:0002687 | positive regulation of leukocyte migration | 2 of 63 | 0.0265 |
| GO:0002548 | monocyte chemotaxis | 2 of 12 | 0.0265 |
| GO:0071347 | cellular response to interleukin-1 | 2 of 75 | 0.0267 |
| GO:0051173 | positive regulation of nitrogen compound metabolic process | 5 of 1184 | 0.0267 |

| (B) KEGG Pathways | Pathway Description | Count in Gene Set | False Discovery Rate |
|---|---|---|---|
| rno04060 | Cytokine–cytokine receptor interaction | 3 of 217 | 0.0130 |

| (C) Reactome Pathways | Pathway Description | Count in Gene Set | False Discovery Rate |
|---|---|---|---|
| RNO-68877 | Mitotic prometaphase | 4 of 168 | 0.00063 |
| RNO-5663220 | RHO GTPases activate formins | 3 of 116 | 0.0013 |
| RNO-2500257 | Resolution of sister chromatid cohesion | 3 of 100 | 0.0013 |
| RNO-141444 | Amplification of signal from unattached kinetochores *via* a MAD2 inhibitory signal | 3 of 80 | 0.0013 |
| RNO-2467813 | Separation of sister chromatids | 3 of 149 | 0.0019 |

## 3. Discussion

### 3.1. Methodology

There are many studies about $TiO_2$ nanoparticles (NP) toxicity. Nevertheless, there are few publications comparing *in vitro* and *in vivo* exposures and even less comparing air–liquid interface exposure with other *in vitro* and *in vivo* exposures. Moreover, the Vitrocell Cloud® system is an innovative system using cloud exposure by a nebulizer, which mimics the lung interface. In this original study we compare the classic *in vitro* method with Vitrocell Cloud® and *in vivo* exposures to $TiO_2$ nanoparticles in a complete transcriptomic study. In the current state of our knowledge, it is the first publication comparing these three expositions methods. Identification of common markers of exposure or effect is relevant for the development of smart and quick tests of nanotoxicity. In addition, in order to respect the three "R" of the ethical approach outlined by Russel and Burch in 1959 to reduce, replace and refine the use of animal testing, it seems relevant to develop *in vitro*

models [37]. It is obvious that the *in vitro* study of different cell lines represents a promising tool for the implementation of predictive devices for NP exposure [38]. Thus, the aim of this study was to identify and validate early specific markers of lung exposure to $TiO_2$ NP, by comparing *in vitro*, air–liquid interface (ALI) and *in vivo* exposures.

Knowing that nanoparticles can reach the alveoli [39], NR8383 cells are an appropriate model because they are alveolar macrophage precursors, which are the first implicated cells in the alveolar clearance of nanoparticles [40–42].

This cell line has already been studied and validated as a model in the field of nanotoxicology [20,43]. Indeed, NR8383 cells are relevant for their immune functions [21]. NR8383 cells were exposed under classic submerged conditions or through an ALI cloud device (Vitrocell Cloud System®), to 3 $cm^2/cm^2$ (19 µg/mL of $TiO_2$ NP) during 4 h.

To limit the bias due to agglomeration of nanoparticles, $TiO_2$ NP were sonicated and vortexed before each treatment. However, typical submerged exposition methods do not take into account the cellular interactions, the role of alveolar surfactant, the pulmonary clearance and the differential deposition in the respiratory tract regarding the displacement of NPs in the air during the respiration [39,44,45]. Moreover, the surfactant plays an important role in the uptake of nanoparticles (Geiser, 2010). Therefore, we chose to compare classic *in vitro* method with ALI exposure using the same cell line, exposed with a nebulizer first to the surfactant and then to $TiO_2$ NP, at the same dose.

The *in vivo* study was carried out on Fischer 344 rats exposed by inhalation (nose only) of 10 $mg/m^3$, 6 h/day, 5 days/week for 4 weeks to $TiO_2$ NP NM-105. Immediately after the last exposure of the rats, the genes expression was analyzed by transcriptomics and compared to *in vitro* results on NR8383 rat macrophages submerges and in air–liquid interface exposure.

### 3.2. Viability of NR8383 Cells Exposed to $TiO_2$

NR8383 cells were exposed to $TiO_2$ NP from 0.25 to 200 µg/mL for 24 h. The viability tests showed a little, although not significant, decrease of mitochondrial activity activity up to 10 % decrease for 100 and 200 µg/mL of NM105 in WST-1 test and for cell membrane integrity up to 30 % decrease for 100 and 200 µg/mL of NM105 in LDH test (Figure 2). The real cytotoxic potential of $TiO_2$ NP remains uncertain and depends on their size, agglomeration and crystalline composition: anatase seems to be less toxic than rutile form [46,47]. In addition, a review reports no reduction in viability for BEAS-2B cells exposed to NM-105 at 150 µg/mL [48]. Another study showed no loss of cell membrane integrity in a 3D human bronchial model exposed to $TiO_2$ NP [49]. At the opposite, Park et al. found a significant loss of 30 % viability, by MTT assay, in BEAS-2B cells exposed to 40 µg/mL of $TiO_2$ NP while Wiemann et al. found a significant loss of cell membrane integrity, by LDH assay, in NR8383 exposed to 90 and 180 µg/mL of NM-105 $TiO_2$ NP: 53.6 % and 69.2 %, respectively [50]. A high toxicity of $TiO_2$ NP was also found in RLE-6TN rat alveolar epithelial cells: IC50 was found to be 7 µg/mL following 24 h exposure [51].

### 3.3. Number of DEGs in Each Exposure Method

The number of differentially expressed genes was higher in *in vitro* submerged model than the others regarding both the number of genes and fold changes (1721 DEGs with a fold change > 3, Table 2), whereas ALI exposure resulted in less differences between exposed and control cells (1 DEG with a fold change > 3, Table 2). Given a fold change > 1.3, the number of genes dysregulated for *in vitro* submerged cells is ten times bigger than the number of genes dysregulated *in vivo* and in ALI conditions: 9836, 851 and 1477, respectively (Table 2). These differences are probably due to the exposition mode and to the cell type model. Indeed, *in vitro* submerged exposure is the common method used in toxicology studies, but it showed some limits: the sedimentation of nanoparticles is heterogenous because of the aqueous behavior, agglomeration, interaction with the solvent and proteins, density, dispersion, dissolution and sedimentation [52–54]. Consequently, the cells can be heterogeneously exposed with some cells exposed in excess and some not exposed at all [53].

High numbers of DEG genes between for *in vitro* submerged cells was already observed in previous transcriptomics studies [55–57]. This is why we chose to focus on DEGs with a FC > 2.8 for *in vitro* submerged exposition.

ALI NR8383 cell culture with surfactant have showed less DEG genes than classic *in vitro* exposed cells without surfactant, this may be explained by the short exposure time and the surfactant layer above cells. Nevertheless, some studies showed that surfactant allows a better uptake of $TiO_2$ nanoparticles by alveolar macrophages. Pulmonary surfactant is composed of phospholipids and lipids (80% and 10%, respectively) and 10% proteins, among them, collectin proteins (SP-A, B, C, D) which rapidly opsonize the particles and modulate the immune response by increasing the macrophages phagocytosis [58,59]. This may suggest that the ALI exposition method with surfactant before $TiO_2$ exposure should have improved the uptake and the cell response and consequently the number of DEG compared to classic *in vitro* exposure without surfactant. But this is not the case in our study, and this implies that other mechanisms could play a role. Opsonization by surfactant proteins is a rapid process that occurs between 5 and 15 min [60], so the time course of opsonization does not seem to be involved in our results.

However, dispersion and settling of NP depend on the pH of surfactant, its composition and its concentration [61,62]. $TiO_2$ dispersion stability and agglomeration depend also on the electronic properties of the surfactant [63,64]. The formation of micelles could lead to the engulfment of NP [65–67] and $TiO_2$ NPs are more electronegative and agglomerate less in electrolytic surfactants [68,69]. Indeed, $TiO_2$ NP dispersion was shown to remain stable in surfactant, but NPs settles easily at the bottom in media without surfactant [61], probably reducing the contact of NPs with cells. As a confirmation, this hypothesis was already observed with other NPs, for example, cells treated four hours with $SiO_2$ NP in the presence of pulmonary surfactant have showed less internalization of NPs, and microscopic observations of the cells showed NPs with less agglomeration and floating above the cell culture [70].

To elucidate the influence of surfactant in macrophages response to $TiO_2$ NPs, it will be crucial to further study the composition of rat surfactant, the turbidity of this surfactant with $TiO_2$, the deposition time of $TiO_2$, and electronic microscopy imaging of NR8383 cells with surfactant exposed to NP $TiO_2$ NM-105 at different time points.

$TiO_2$ NP was a mixed phase nanocrystalline powder composed of approximately 80% anatase and 20% rutile, with an average primary particle diameter of 21.5 ± 7.2 nm (Table 1). $TiO_2$ aerosol was generated at a target concentration of 10 mg/m$^3$. Taking into account the interspecies differences in terms of respiratory parameters and lung deposited dose, this concentration and exposure time relate to the 8 h weighted average occupational exposure of a worker at 0.3 mg/m$^3$ during most of its career, the NIOSH recommended exposure limit for ultrafine $TiO_2$ [71,72].

In a concomitant study realized with F344 rats, at the end of the inhalation period, the concentration of titanium in lung tissue was approximately 2 mg/lung in exposed rats [73]. In the lung, after inhalation, the particles are preferentially deposited in the proximal alveolar region (PAR). Then, the surface area of particles per unit area of PAR is approximately 5 cm$^2$/cm$^2$ [73] while the threshold dose for the onset of inflammation is estimated at approximately 1 cm$^2$/cm$^2$ [74]. The presence of a strong pulmonary inflammation at the end of the exposure, agrees with these data. Finally, the presence of macrophages loaded with $TiO_2$ NP in the alveoli and the lymph nodes associated with the lungs [22], suggests a conservation of the mechanisms of particle elimination, by the mucociliary escalator or by translocation from the alveolar region to the lymph nodes. These results demonstrate the key role of alveolar macrophages in the pulmonary response to nanoparticle inhalation and justify the comparison of *in vivo* response with that of cultured rat alveolar macrophages.

### 3.4. Transcriptomic Study

The analysis of the 20 most up-DEG and 20 most down-DEG in the three conditions highlights five KEGG pathways dysregulated for *in vitro* submerged cells exposed to $TiO_2$ NP including 'IL-17 signaling pathway', 'chemokine signaling pathway' and 'cytokine–cytokine receptor interaction'.

Interestingly, 'Il-17 signaling pathway' is commonly associated with the activity of T lymphocytes, but macrophages were already demonstrated to be involved in Il-17 mediated inflammation as suggested by the (*i*) upregulation of IL17 receptors in vitro, (*ii*) their production of unique profiles of cytokines and chemokines [75] and (*iii*) the activation of macrophages in a M1/M2 heterogeneous phenotype [76]. Five common biologic process (GO-BP) were found between *in vivo* and ALI exposures, only one between *in vivo* and *in vitro* exposures and none between ALI and *in vitro* exposures. The 5 common GO-BP are involved in metabolic and cellular processes, suggesting that cellular responses in ALI conditions are similar to those obtained for *in vivo* condition.

GSEA analysis highlighted two common gene sets dysregulated in all three exposure, related to inflammation and oncogenesis: the IL6-JAK-STAT3 signaling and genes regulated by the transcription factor MYC (MYC_TARGETS_V2) (Table 3). IL6-JAK-STAT3 pathway is known to be implied in tumorigenesis [77] and play a role in cancer-associated inflammatory environment [78] and angiogenesis [79]. Genes regulated by the transcription factor *Myc* are mainly involved in cell growth, apoptosis and metabolism. The *Myc* gene is well known as a proto-oncogene that is over expressed in various types of cancers include lymphomas, lung carcinoma, breast carcinoma and colon carcinomas [80]. *Myc* is also known to be involved in the polarization of M2 tumor-associated macrophages and is targeted for new therapeutic strategies against cancer [81–84].

Interestingly, as opposed to what could be expected, *Myc* was the most downregulated gene in ALI exposures (Table 2). However, the role of this transcription factor is large and remain poorly understood. Some studies have shown that downregulation of *Myc* gene can induce cell cycle arrest and, in some case cell survival, differentiation or apoptosis [85–87]. As no cell death was observed after NM105 TiO$_2$ NP exposure in our study, we can suppose that the down regulation of *Myc* in NR8383 exposed in ALI experiments, may be associated with a cell cycle arrest and survival of NR8383. Cell survival and cell cycle states in these conditions will be further investigated.

To propose biomarkers of effect for NM-105 TiO$_2$, we focused our analyses on the common dysregulated genes (DEGs) between the three exposure modes. 18 common DEGs were found, among them, only 4 are upregulated in the three conditions: *Ccl4*, Ccl7, *Osm* and *Bcl3*, while the other common DEG display a non-homogenous dysregulation. Indeed, among the 18 DEGs, 14 DEGs showed the same dysregulation profile following *in vitro* and ALI conditions: among them 12 DEGs were down regulated and 2 upregulated as noted in Table 4. Contrary those genes were downregulated *in vivo*. Only *Ptpn13* was downregulated *in vivo* and in ALI conditions while upregulated *in vitro* (see Table 4). These discordant results can be explained by the experiments conditions. For *in vivo* study, transcriptomic analyses consider all the cellular perturbations induced by NP exposure as well as the interaction between the different cell types including macrophages, epithelial, interstitial and endothelial cells, after a subacute exposure (6 h/day, 5 days/week for 4 weeks) while only NR8383 cells are grown for a short 4 h exposure in both vitro tests. Moreover, surfactant was present in ALI and *in vivo* conditions, but not for *in vitro* submerged conditions.

Consistently with our previous observations, common dysregulations for *in vitro* and ALI *versus in vivo* exposures revealed a negative regulation of mitosis and cell proliferation and a negative regulation of M2 polarization of macrophages (Table 4). These observations are in accordance with the hypothesis of a cell cycle arrest without any cytotoxicity of macrophages *in vitro* and in ALI conditions. It can be an early effect of TiO$_2$ NP on macrophages, while the upregulation of these genes for *in vivo* conditions can be due to other cell types in lung or to an adaptive regulation towards proliferation after a longer *in vivo* exposure.

Note that macrophages are ubiquitous innate immune cells and can be polarized in two distinct functional phenotypes, either in pro-inflammatory macrophages called M1 or in M2 macrophages that promote immune suppression and wound healing [88–90]. They also suggest a preferential differentiation in M2 macrophages *in vivo* compared to M1 that were found *in vitro* and in ALI conditions. It is well known that in cancer pathologies, M2 macrophages can be recruited and favor tumor growth by contributing to the tumor microenvironment; by the way, they are called

tumor-associated macrophages (TAM). Furthermore, *Ptpn13* is a tumor suppressor gene that is frequently inactivated in non–small cell lung cancer (NSLC) (in more than 70% of NSLC) [91], and was downregulated in our ALI and *in vivo* exposure to TiO$_2$ while upregulated in *in vitro* condition.

The four genes upregulated in the three exposure conditions are actor of the cytokine–cytokine receptor interaction KEGG pathway: *Ccl4*, CcL7, *Osm* and *Bcl3* is implied in cell proliferation regulation (Table 4). Interestingly, *Ccl4* was already identified as a candidate for biomarker for BCR pathway activation and prognostic in diffuse large B cell lymphoma [92] and as an inflammation-related diseases biomarker (Olink proteomics). *Ccl7* (also called *MCP3*) plays a crucial role in cancer as it can promote tumor growth, tumor microenvironment, invasion and metastasis [93]. Indeed, overexpression of *Ccl7* was associated with lung adenomas [94] and metastasis in colorectal cancer and renal carcinoma [95–97]. Moreover, *Ccl7* expression is associated with the recruitment of tumor-associated macrophages (TAMs) [98]. Likewise, oncostatin M (*Osm*) is identified as an inflammation biomarker in periodontal diseases [99], sepsis [100], inflammatory bowel disease [101,102]. Other studies showed that *Osm* promotes cancer cell plasticity [103] and the polarization of pro-fibrotic M2-like macrophages [104]. Finally, *Bcl3* (B-cell lymphoma 3 gene) is a proto-oncogene whose product is an inhibitor of *NF-kappa B* [105,106] and display anti-apoptotic functions. *Bcl3* is involved in some cancers, the most known is his role in lymphoma, in which he regulates pro-survival and pro-inflammatory gene expression [107]. *Bcl3* is also involved in solid tumor progression [108] like ovarian [109], cervical cancers [110,111], mammary cancer metastasis [112] and tumor progression in breast cancer [113]. In macrophages, *Bcl3* was showed to be a key mediator of IL-10 macrophage polarization to an immunosuppressive phenotype as observed in TAM [88].

## 4. Materials and Methods

### *4.1. TiO$_2$ NP Characterization*

TiO$_2$ NP mainly composed of anatase and rutile (82:18) were obtained by the Joint Research Center (NM-105, JRC). TiO$_2$ were resuspended in ultrapure water (18 mΩ) at a concentration of 2.56 mg/mL [114], then directly sonicated (Vibracell 75022, Bioblock, Illkirch-Graffenstaden, France) at a magnitude of 30%, during 6 min under a permanent cooling. After the sonication, TiO$_2$ NP were diluted at a 6.25 μg/mL in DMEM-SVF free cell culture medium (Sigma-Aldrich, Saint-Louis, MO, USA). NP morphology was observed by transmission electronic microscope (TEM). The hydrodynamic diameter and the polydispersity index were measured by dynamic light diffusion (DLS, ZetasizerTM3000E, Malvern Instruments, Worcestershire, UK). The *zeta* potential was measured by Smoluchowski's equation [115].

### *4.2. Cell Culture*

NR8383 cells were obtained from the ATCC (American Type Culture Collection, Manassas, VA, USA). Cells were cultured in DMEM medium completed by 15% of fetal bovine serum (FBS), 100 U/mL of penicillin, 100 μg/mL of streptomycin, 0.25 μg/mL of amphotericin and 2 mM of L-glutamine at a 37 °C temperature and under a 5 % CO$_2$ atmosphere. For all tests, the density used was of $5 \times 10^4$ cells/mL.

### *4.3. In Vitro Cytotoxicity Study*

Cell viability was assessed with the WST-1 assay and the measure of the lactate dehydrogenase (LDH) release in the extracellular medium. Non-exposed cells were considered as a control. Six technical and four biologic replicates were used per each condition. After a 24-h exposure to TiO$_2$ NP, cells were incubated with 5% of WST-1, during 2 h at 37 °C. Then, absorbance was measured at 450 nm, with a 690 nm as reference wavelength (iMarkTM, Bio-Rad). LDH dosage was carried out following manufacturer's recommendations. Briefly, after 24 h of exposure to TiO$_2$ NP, cells were incubated 30 min with 100 μL of mix of LDH buffer and substrate, at 20 °C. Then, 50 μL of stop solution were

added and the absorbance was measured at 490 nm (iMarkTM, Bio-Rad). The positive control was the result of cells exposed to the lysis buffer (Triton 5%) during 15 min before the measure. Data are presented as means ± standard deviation (SD) of the four biologic replicates. Statistical differences were determined by a one-way analysis of variance (one-way ANOVA) followed by the post hoc Dunnett's test.

### 4.4. In Vivo Exposure

The animal experiments were performed according to European (Directive 2010/63/EC) and French (Décret n°2013-118) legislations regarding the protection of animals used for scientific purposes. The INRS animal facility has full accreditation (authorization n°D54-547-10) from the French Ministry of Agriculture. This study was approved on October 14th, 2013 by the regional ethical committee (CELMEA n°066) appointed by the Ministry of higher education and research (Authorization n°00692.01).

The *in vivo* exposure was made at the National Institute for Research and Safety (INRS) and described previously [22]. Briefly, thirteen-week-old male Fisher F344 rats (Charles River Laboratories, France) were housed in standard environmental conditions (relative humidity: 55 ± 10 %; temperature: 22 ± 2 °C and 12/ 12 h light/dark cycle). Water and a standard laboratory animal diet (A04, Safe diet) were freely available. Two weeks before exposure, rats were gradually acclimatized to the restraining tubes. Animals were then exposed by nose-only inhalation either to filtered air (controls) or $TiO_2$ aerosol at a concentration of 10 mg/$m^3$ for 6 h/day, 5 days/week for 4 weeks. Immediately after the exposure period, the animals were anesthetized with pentobarbital (60 mg/kg) and exsanguinated through the abdominal aorta and lung tissues were collected. Gene expression was analyzed by transcriptomic analysis on the entire pulmonary accessory lobe. We reanalyzed the transcriptomic results obtained *in vivo* (GEO Accession: GSE99997) [22] in order to compare them with the results obtained *in vitro* and in ALI conditions.

### 4.5. Exposure at the Air–liquid Interface

Cells in air–liquid interface were exposed to aerosolized NM-105 nanoparticles using the Vitrocell cloud System®. ALI exposure methodology used here is described in detail in another study [116]. Briefly, NR8383 were seeded in Transwell® culture inserts (Polyester membrane, TC-treated, Corning, USA) with 300.000 cells/insert during 24 h before air–liquid interface exposure with the nebulization of pig surfactant and then NM-105 NP. After exposure to 3 $cm^2$ of $TiO_2$ NP/$cm^2$ of cell culture, cells were incubated 4 h in a 37 °C, under a 5% $CO_2$ atmosphere, and RNA extractions were performed.

### 4.6. Transcriptomic Study

*Total RNA Extraction.* In order to evaluate gene expression profile, total RNA was extracted from NM-105 exposed cells during 4 h at 3 $cm^2$ of $TiO_2$ NP/$cm^2$ of cell culture (same dose for ALI and submerged experiments), using RNA-Solv (R6830-02, USA). The unexposed cells were used as a control. The RNA concentration was determined by measuring the absorption at 260 nm using a spectrophotometer (Biotech-BioSpec-Nano, Shimadzu). The optimal purity of the RNA was ensured by the determination of 260/280 nm of an absorbance ratio A260/A280 > 1.8. RNA integrity was confirmed with the Agilent 2100 and RNA 6000 Nano LabChip bioanalyzer kits (Agilent Biotechnologies, Palo Alto, CA, USA). The threshold of 8 for RNA integrity number (RIN) was chosen as a cutoff to determine whether the extracted RNA was qualified or not.

*Expression microarray hybridization.* One hundred nanograms of RNA from each sample was labeled with cyanine 3-CTP using the low input quick amp labeling kit (Agilent Technologies). The labeled cRNAs were purified and hybridized on the Agilent G4853A Sure Print G3 Rat GE 8 * 60 K microarray chips (Agilent Technologies) that cover the entire rat transcriptome. The slides were then washed and scanned using the Agilent G2505C microarray scanner with a resolution of 3 μm. The data were extracted using Feature Extraction software version 11.0 (Agilent).

*Bioinformatics analyses.* First, the data were standardized using the GeneSpring software. The Student's test followed by the Benjamini–Hochberg correction and the filtering criteria were applied, to identify the genes whose level of expression was considerably modified. Genes with expression changes at a fold change (FC) > |1.5| compared to control with $p < 0.05$ were considered differentially expressed at a significant level. Genes were clustered into groups according to different criteria, such as the terms gene ontology (GO) biologic process and pathways (KEGG and Reactome) (see Table 3). Gene Set Enrichment Analysis (GSEA) functional annotation was done from MSigDB Collections. For biologic interpretation, we considered the GO biologic process and pathways with a $p \leq 0.05$ value in the cluster with an enrichment score (Z-score) greater than 1.3 [117]. Venn diagram were realized thanks to GeneVenn online software [118]. The heatmap was realized with ClustVis software online [119].

## 5. Conclusions

This work suggests that *Ccl4*, *Osm*, *Ccl7* and *Bcl3*, are early response biomarkers to TiO$_2$ NP. Interestingly, *Ccl7* and *Bcl3* genes were predicted as biomarkers of TiO$_2$ effects using a machine learning approach and mice *in vivo* datasets by our colleagues within the SmartNanotox project (preliminary results, Vadim Zhernovkov). This analysis permits us to identify five common GO-BP between *in vivo* and ALI exposures and only one between submerged and *in vivo*, suggesting that ALI better reflects the effect of TiO$_2$ NP exposure *in vivo*. It could be interesting, in a future work, to assess other nanoobjects, such as metal oxides or carbonaceous, to verify if these genes are modified too, suggesting a "nano" effect or if not, validating a specific titanium oxide response.

Thus, this work justifies the pertinence of our *in vitro* models, which, regardless of ethical considerations, are cost and time effective, as *in vivo* experiments could produce valuable results in 8 months and *in vitro* within two weeks.

## References

1. Jaroenworaluck, A.; Sunsaneeyametha, W.; Kosachan, N.; Stevens, R. Characteristics of silica-coated TiO2 and its UV absorption for sunscreen cosmetic applications. *Surf. Interface Anal.* **2006**, *38*, 473–477. [CrossRef]
2. Weir, A.; Westerhoff, P.; Fabricius, L.; Hristovski, K.; von Goetz, N. Titanium Dioxide Nanoparticles in Food and Personal Care Products. *Environ. Sci. Technol.* **2012**, *46*, 2242–2250. [CrossRef] [PubMed]
3. Ahn, T.-K.; Lee, D.H.; Kim, T.; Jang, G.C.; Choi, S.; Oh, J.B.; Ye, G.; Lee, S. Modification of Titanium Implant and Titanium Dioxide for Bone Tissue Engineering. In *Novel Biomaterials for Regenerative Medicine*; Chun, H.J., Park, K., Kim, C.-H., Khang, G., Eds.; Springer: Singapore, 2018; Volume 1077, pp. 355–368. ISBN 9789811309465.
4. Shi, H.; Magaye, R.; Castranova, V.; Zhao, J. Titanium dioxide nanoparticles: A review of current toxicological data. *Part. Fibre Toxicol.* **2013**, *10*, 15. [CrossRef] [PubMed]

5.	Ziental, D.; Czarczynska-Goslinska, B.; Mlynarczyk, D.T.; Glowacka-Sobotta, A.; Stanisz, B.; Goslinski, T.; Sobotta, L. Titanium Dioxide Nanoparticles: Prospects and Applications in Medicine. *Nanomaterials* **2020**, *10*, 387. [CrossRef] [PubMed]

6.	Howarter, J.A.; Youngblood, J.P. Self-Cleaning and Next Generation Anti-Fog Surfaces and Coatings. *Macromol. Rapid Commun.* **2008**, *29*, 455–466. [CrossRef]

7.	Li, S.-X.; Lin, X.; Zheng, F.-Y.; Liang, W.; Zhong, Y.; Cai, J. Constituting Fully Integrated Visual Analysis System for Cu(II) on TiO2 /Cellulose Paper. *Anal. Chem.* **2014**, *86*, 7079–7083. [CrossRef]

8.	Markowska-Szczupak, A.; Ulfig, K.; Grzmil, B.; Morawski, A. A preliminary study on antifungal effect of TiO2-based paints in natural indoor light. *Pol. J. Chem. Technol.* **2010**, *12*, 53–57. [CrossRef]

9.	Rathee, D.; Arya, S.K.; Kumar, M. Analysis of TiO2 for microelectronic applications: Effect of deposition methods on their electrical properties. *Front. Optoelectron. China* **2011**, *4*, 349–358. [CrossRef]

10.	Wu, M.J.; Bak, T.; O'Doherty, P.J.; Moffitt, M.C.; Nowotny, J.; Bailey, T.D.; Kersaitis, C. Photocatalysis of Titanium Dioxide for Water Disinfection: Challenges and Future Perspectives. *Int. J. Photochem.* **2014**, *2014*, 1–9. [CrossRef]

11.	Armand, L.; Tarantini, A.; Beal, D.; Biola-Clier, M.; Bobyk, L.; Sorieul, S.; Pernet-Gallay, K.; Marie-Desvergne, C.; Lynch, I.; Herlin-Boime, N.; et al. Long-term exposure of A549 cells to titanium dioxide nanoparticles induces DNA damage and sensitizes cells towards genotoxic agents. *Nanotoxicology* **2016**, *10*, 913–923. [CrossRef] [PubMed]

12.	Johnston, H.J.; Hutchison, G.R.; Christensen, F.M.; Peters, S.; Hankin, S.; Stone, V. Identification of the mechanisms that drive the toxicity of TiO(2)particulates: The contribution of physicochemical characteristics. *Part. Fibre Toxicol.* **2009**, *6*, 33. [CrossRef] [PubMed]

13.	Landsiedel, R.; Ma-Hock, L.; Hofmann, T.; Wiemann, M.; Strauss, V.; Treumann, S.; Wohlleben, W.; Gröters, S.; Wiench, K.; van Ravenzwaay, B. Application of short-term inhalation studies to assess the inhalation toxicity of nanomaterials. *Part. Fibre Toxicol.* **2014**, *11*, 16. [CrossRef] [PubMed]

14.	Li, Y.; Yan, J.; Ding, W.; Chen, Y.; Pack, L.M.; Chen, T. Genotoxicity and gene expression analyses of liver and lung tissues of mice treated with titanium dioxide nanoparticles. *Mutagenesis* **2017**, *32*, 33–46. [CrossRef] [PubMed]

15.	Cui, Y.; Gong, X.; Duan, Y.; Li, N.; Hu, R.; Liu, H.; Hong, M.; Zhou, M.; Wang, L.; Wang, H.; et al. Hepatocyte apoptosis and its molecular mechanisms in mice caused by titanium dioxide nanoparticles. *J. Hazard. Mater.* **2010**, *183*, 874–880. [CrossRef]

16.	Cui, Y.; Liu, H.; Ze, Y.; Zengli, Z.; Hu, Y.; Cheng, Z.; Cheng, J.; Hu, R.; Gao, G.; Wang, L.; et al. Gene expression in liver injury caused by long-term exposure to titanium dioxide nanoparticles in mice. *Toxicol. Sci. Off. J. Soc. Toxicol.* **2012**, *128*, 171–185. [CrossRef]

17.	Lenz, A.G.; Karg, E.; Lentner, B.; Dittrich, V.; Brandenberger, C.; Rothen-Rutishauser, B.; Schulz, H.; Ferron, G.A.; Schmid, O. A Dose-Controlled System for Air-Liquid Interface Cell Exposure and Application to Zinc Oxide Nanoparticles. *Part. Fibre Toxicol.* **2009**, *6*, 32. [CrossRef]

18.	Lenz, A.-G.; Karg, E.; Brendel, E.; Hinze-Heyn, H.; Maier, K.L.; Eickelberg, O.; Stoeger, T.; Schmid, O. Inflammatory and Oxidative Stress Responses of an Alveolar Epithelial Cell Line to Airborne Zinc Oxide Nanoparticles at the Air-Liquid Interface: A Comparison with Conventional, Submerged Cell-Culture Conditions. *Biomed Res. Int.* **2013**, *2013*, 652632. [CrossRef]

19.	Lenz, A.-G.; Stoeger, T.; Cei, D.; Schmidmeir, M.; Semren, N.; Burgstaller, G.; Lentner, B.; Eickelberg, O.; Meiners, S.; Schmid, O. Efficient Bioactive Delivery of Aerosolized Drugs to Human Pulmonary Epithelial Cells Cultured in Air-Liquid Interface Conditions. *Am. J. Respir. Cell Mol. Biol.* **2014**, *51*, 526–535. [CrossRef] [PubMed]

20.	Eidi, H.; Joubert, O.; Némos, C.; Grandemange, S.; Mograbi, B.; Foliguet, B.; Tournebize, J.; Maincent, P.; Le Faou, A.; Aboukhamis, I.; et al. Drug delivery by polymeric nanoparticles induces autophagy in macrophages. *Int. J. Pharm.* **2012**, *422*, 495–503. [CrossRef]

21.	Hussain, S.; Vanoirbeek, J.A.J.; Hoet, P.H.M. Interactions of nanomaterials with the immune system. *WIREs Nanomed. Nanobiotechnol.* **2012**, *4*, 169–183. [CrossRef]

22.	Chézeau, L.; Sébillaud, S.; Safar, R.; Seidel, C.; Dembélé, D.; Lorcin, M.; Langlais, C.; Grossmann, S.; Nunge, H.; Michaux, S.; et al. Short- and long-term gene expression profiles induced by inhaled TiO2 nanostructured aerosol in rat lung. *Toxicol. Appl. Pharmacol.* **2018**, *356*, 54–64. [CrossRef] [PubMed]

23. Volkov, V.A.; Grissom, P.M.; Arzhanik, V.K.; Zaytsev, A.V.; Renganathan, K.; McClure-Begley, T.; Old, W.M.; Ahn, N.; McIntosh, J.R. Centromere protein F includes two sites that couple efficiently to depolymerizing microtubules. *J. Cell Biol.* **2015**. [CrossRef] [PubMed]

24. McCleland, M.L.; Gardner, R.D.; Kallio, M.J.; Daum, J.R.; Gorbsky, G.J.; Burke, D.J.; Stukenberg, P.T. The highly conserved Ndc80 complex is required for kinetochore assembly, chromosome congression, and spindle checkpoint activity. *Genes Dev.* **2003**, *17*, 101–114. [CrossRef] [PubMed]

25. Tanenbaum, M.E.; Macůrek, L.; Janssen, A.; Geers, E.F.; Alvarez-Fernández, M.; Medema, R.H. Kif15 cooperates with eg5 to promote bipolar spindle assembly. *Curr. Biol. CB* **2009**, *19*, 1703–1711. [CrossRef]

26. Mi, Y.; Zhang, C.; Bu, Y.; Zhang, Y.; He, L.; Li, H.; Zhu, H.; Li, Y.; Lei, Y.; Zhu, J. DEPDC1 is a novel cell cycle related gene that regulates mitotic progression. *BMB Rep.* **2015**, *48*, 413–418. [CrossRef]

27. Pallier, C.; Scaffidi, P.; Chopineau-Proust, S.; Agresti, A.; Nordmann, P.; Bianchi, M.E.; Marechal, V. Association of Chromatin Proteins High Mobility Group Box (HMGB) 1 and HMGB2 with Mitotic Chromosomes. *Mol. Biol. Cell* **2003**, *14*, 3414–3426. [CrossRef]

28. Wang, W.; Jiang, H.; Zhu, H.; Zhang, H.; Gong, J.; Zhang, L.; Ding, Q. Overexpression of high mobility group box 1 and 2 is associated with the progression and angiogenesis of human bladder carcinoma. *Oncol. Lett.* **2013**, *5*, 884–888. [CrossRef]

29. Kwon, J.-H.; Kim, J.; Park, J.Y.; Hong, S.M.; Park, C.W.; Hong, S.J.; Park, S.Y.; Choi, Y.J.; Do, I.-G.; Joh, J.-W.; et al. Overexpression of High-Mobility Group Box 2 Is Associated with Tumor Aggressiveness and Prognosis of Hepatocellular Carcinoma. *Clin. Cancer Res.* **2010**. [CrossRef]

30. Hechler, B.; Gachet, C. P2 receptors and platelet function. *Purinergic Signal.* **2011**, *7*, 293–303. [CrossRef]

31. Zhu, C.; Kros, J.M.; van der Weiden, M.; Zheng, P.; Cheng, C.; Mustafa, D.A.M. Expression site of P2RY12 in residential microglial cells in astrocytomas correlates with M1 and M2 marker expression and tumor grade. *Acta Neuropathol. Commun.* **2017**, *5*, 4. [CrossRef]

32. Wang, Y.; Zhu, J.; Zhang, L.; Zhang, Z.; He, L.; Mou, Y.; Deng, Y.; Cao, Y.; Yang, P.; Su, Y.; et al. Role of C/EBP homologous protein and endoplasmic reticulum stress in asthma exacerbation by regulating the IL-4/signal transducer and activator of transcription 6/transcription factor EC/IL-4 receptor α positive feedback loop in M2 macrophages. *J. Allergy Clin. Immunol.* **2017**, *140*, 1550–1561.e8. [CrossRef]

33. Rehli, M.; Sulzbacher, S.; Pape, S.; Ravasi, T.; Wells, C.A.; Heinz, S.; Söllner, L.; Chartouni, C.E.; Krause, S.W.; Steingrimsson, E.; et al. Transcription Factor Tfec Contributes to the IL-4-Inducible Expression of a Small Group of Genes in Mouse Macrophages Including the Granulocyte Colony-Stimulating Factor Receptor. *J. Immunol.* **2005**, *174*, 7111–7122. [CrossRef] [PubMed]

34. Yanagawa, T.; Sumiyoshi, H.; Higashi, K.; Nakao, S.; Higashiyama, R.; Fukumitsu, H.; Minakawa, K.; Chiba, Y.; Suzuki, Y.; Sumida, K.; et al. Identification of a Novel Bone Marrow Cell-Derived Accelerator of Fibrotic Liver Regeneration Through Mobilization of Hepatic Progenitor Cells in Mice. *STEM CELLS* **2019**, *37*, 89–101. [CrossRef] [PubMed]

35. Zhang, Q.; Li, H.; Mao, Y.; Wang, X.; Zhang, X.; Yu, X.; Tian, J.; Lei, Z.; Li, C.; Han, Q.; et al. Apoptotic SKOV3 cells stimulate M0 macrophages to differentiate into M2 macrophages and promote the proliferation and migration of ovarian cancer cells by activating the ERK signaling pathway. *Int. J. Mol. Med.* **2019**. [CrossRef] [PubMed]

36. Yamashita, H.; Shuman, L.; Warrick, J.I.; Raman, J.D.; Degraff, D.J. Androgen represses opioid growth factor receptor (OGFR) in human prostate cancer LNCaP cells and OGFR expression in human prostate cancer tissue. *Am. J. Clin. Exp. Urol.* **2018**, *6*, 164–171.

37. Tannenbaum, J.; Bennett, B.T. Russell and Burch's 3Rs then and now: The need for clarity in definition and purpose. *J. Am. Assoc. Lab. Anim. Sci. JAALAS* **2015**, *54*, 120–132.

38. Alhadlaq, H.A.; Akhtar, M.J.; Ahamed, M. Zinc ferrite nanoparticle-induced cytotoxicity and oxidative stress in different human cells. *Cell Biosci.* **2015**, *5*. [CrossRef]

39. Oberdörster, G.; Oberdörster, E.; Oberdörster, J. Nanotoxicology: An Emerging Discipline Evolving from Studies of Ultrafine Particles. *Environmental Health Perspectives* **2005**, *113*, 823–839. [CrossRef]

40. Geiser, M. Update on Macrophage Clearance of Inhaled Micro- and Nanoparticles. *J. Aerosol Med. Pulm. Drug Deliv.* **2010**, *23*, 207–217. [CrossRef]

41. Lehnert, B.E. Pulmonary and thoracic macrophage subpopulations and clearance of particles from the lung. *Environ. Health Perspect.* **1992**, *97*, 17–46. [CrossRef]

42. Semmler-Behnke, M.; Takenaka, S.; Fertsch, S.; Wenk, A.; Seitz, J.; Mayer, P.; Oberdörster, G.; Kreyling, W.G. Efficient Elimination of Inhaled Nanoparticles from the Alveolar Region: Evidence for Interstitial Uptake and Subsequent Reentrainment onto Airways Epithelium. *Environ. Health Perspect.* **2007**, *115*, 728–733. [CrossRef] [PubMed]

43. Eidi, H.; Joubert, O.; Attik, G.; Duval, R.E.; Bottin, M.C.; Hamouia, A.; Maincent, P.; Rihn, B.H. Cytotoxicity assessment of heparin nanoparticles in NR8383 macrophages. *Int. J. Pharm.* **2010**, *396*, 156–165. [CrossRef] [PubMed]

44. Islam, M.S.; Paul, G.; Ong, H.X.; Young, P.M.; Gu, Y.T.; Saha, S.C. A Review of Respiratory Anatomical Development, Air Flow Characterization and Particle Deposition. *IJERPH* **2020**, *17*, 380. [CrossRef] [PubMed]

45. Heyder, J. Deposition of Inhaled Particles in the Human Respiratory Tract and Consequences for Regional Targeting in Respiratory Drug Delivery. *Proc. Am. Thorac. Soc.* **2004**, *1*, 315–320. [CrossRef]

46. Gerloff, K.; Fenoglio, I.; Carella, E.; Kolling, J.; Albrecht, C.; Boots, A.W.; Förster, I.; Schins, R.P.F. Distinctive Toxicity of TiO2 Rutile/Anatase Mixed Phase Nanoparticles on Caco-2 Cells. *Chem. Res. Toxicol.* **2012**, *25*, 646–655. [CrossRef]

47. Uboldi, C.; Urbán, P.; Gilliland, D.; Bajak, E.; Valsami-Jones, E.; Ponti, J.; Rossi, F. Role of the crystalline form of titanium dioxide nanoparticles: Rutile, and not anatase, induces toxic effects in Balb/3T3 mouse fibroblasts. *Toxicol. In Vitro* **2016**, *31*, 137–145. [CrossRef]

48. Huang, Y.-W.; Wu, C.; Aronstam, R.S. Toxicity of Transition Metal Oxide Nanoparticles: Recent Insights from *in vitro* Studies. *Materials* **2010**, *3*, 4842–4859. [CrossRef]

49. Haase, A.; Dommershausen, N.; Schulz, M.; Landsiedel, R.; Reichardt, P.; Krause, B.-C.; Tentschert, J.; Luch, A. Genotoxicity testing of different surface-functionalized SiO2, ZrO2 and silver nanomaterials in 3D human bronchial models. *Arch. Toxicol.* **2017**, *91*, 3991–4007. [CrossRef]

50. Wiemann, M.; Vennemann, A.; Sauer, U.G.; Wiench, K.; Ma-Hock, L.; Landsiedel, R. An *in vitro* alveolar macrophage assay for predicting the short-term inhalation toxicity of nanomaterials. *J. Nanobiotechnol.* **2016**, *14*, 16. [CrossRef]

51. Karkossa, I.; Bannuscher, A.; Hellack, B.; Bahl, A.; Buhs, S.; Nollau, P.; Luch, A.; Schubert, K.; von Bergen, M.; Haase, A. An in-depth multi-omics analysis in RLE-6TN rat alveolar epithelial cells allows for nanomaterial categorization. *Part. Fibre Toxicol.* **2019**, *16*, 38. [CrossRef]

52. Cohen, J.M.; Teeguarden, J.G.; Demokritou, P. An integrated approach for the *in vitro* dosimetry of engineered nanomaterials. *Part. Fibre Toxicol.* **2014**, *11*, 20. [CrossRef] [PubMed]

53. Moore, T.L.; Urban, D.A.; Rodriguez-Lorenzo, L.; Milosevic, A.; Crippa, F.; Spuch-Calvar, M.; Balog, S.; Rothen-Rutishauser, B.; Lattuada, M.; Petri-Fink, A. Nanoparticle administration method in cell culture alters particle-cell interaction. *Sci. Rep.* **2019**, *9*, 900. [CrossRef]

54. Thomas, D.G.; Smith, J.N.; Thrall, B.D.; Baer, D.R.; Jolley, H.; Munusamy, P.; Kodali, V.; Demokritou, P.; Cohen, J.; Teeguarden, J.G. ISD3: A particokinetic model for predicting the combined effects of particle sedimentation, diffusion and dissolution on cellular dosimetry for *in vitro* systems. *Part. Fibre Toxicol.* **2018**, *15*, 6. [CrossRef] [PubMed]

55. Doumandji, Z.; Safar, R.; Lovera-Leroux, M.; Nahle, S.; Cassidy, H.; Matallanas, D.; Rihn, B.H.; Ferrari, L.; Joubert, O. Protein and lipid homeostasis altered in rat macrophages after exposure to metallic oxide nanoparticles. *Cell Biol. Toxicol.* **2019**. [CrossRef]

56. Hans, C.P.; Sharma, N.; Sen, S.; Zeng, S.; Dev, R.; Jiang, Y.; Mahajan, A.; Joshi, T. Transcriptomics Analysis Reveals New Insights into the Roles of Notch1 Signaling on Macrophage Polarization. *Sci. Rep.* **2019**, *9*, 7999. [CrossRef] [PubMed]

57. Nahle, S.; Cassidy, H.; Leroux, M.M.; Mercier, R.; Ghanbaja, J.; Doumandji, Z.; Matallanas, D.; Rihn, B.H.; Joubert, O.; Ferrari, L. Genes expression profiling of alveolar macrophages exposed to non-functionalized, anionic and cationic multi-walled carbon nanotubes shows three different mechanisms of toxicity. *J. Nanobiotechnol.* **2020**, *18*, 36. [CrossRef] [PubMed]

58. Sano, H.; Kuroki, Y. The lung collectins, SP-A and SP-D, modulate pulmonary innate immunity. *Mol. Immunol.* **2005**, *42*, 279–287. [CrossRef] [PubMed]

59. Stringer, B.; Kobzik, L. Alveolar macrophage uptake of the environmental particulate titanium dioxide: Role of surfactant components. *Am. J. Respir. Cell Mol. Biol.* **1996**, *14*, 155–160. [CrossRef]

60. Tofte, R.W.; Peterson, P.K.; Kim, Y.; Quie, P.G. Influence of serum concentration on opsonization by the classical and alternative complement pathways. *Infect. Immun.* **1980**, *27*, 693–696. [CrossRef]

61. Che Hak, C.R.; Fatanah, D.N.E.; Abdullah, Y.; Meor Sulaiman, M.Y. The Effect of Surfactants on the Stability of TiO2 Aqueous Suspension. *Int. J. Curr. Res. Sci. Eng. Technol.* **2018**, *1*, 172. [CrossRef]

62. Sato, T.; Kohnosu, S. Effect of surfactant concentration on the stability of aqueous titanium dioxide suspensions. *J. Colloid Interface Sci.* **1991**, *143*, 434–439. [CrossRef]

63. Heijman, S.G.J.; Stein, H.N. Electrostatic and Sterical Stabilization of TiO2 Dispersions. *Langmuir* **1995**, *11*, 422–427. [CrossRef]

64. Tkachenko, N.H.; Yaremko, Z.M.; Bellmann, C.; Soltys, M.M. The influence of ionic and nonionic surfactants on aggregative stability and electrical surface properties of aqueous suspensions of titanium dioxide. *J. Colloid Interface Sci.* **2006**, *299*, 686–695. [CrossRef] [PubMed]

65. Cao, H.; Zhang, X.; Ding, B.; Wang, L.; Lu, N. Synergistic action of TiO $_2$ particles and surfactants on the foamability and stabilization of aqueous foams. *RSC Adv.* **2017**, *7*, 44972–44978. [CrossRef]

66. Gehr, P.; Schürch, S.; Berthiaume, Y.; Hof, V.I.; Geiser, M. Particle Retention in Airways by Surfactant. *J. Aerosol Med.* **1990**, *3*, 27–43. [CrossRef]

67. Imae, T.; Hasegawa, E.; Iwamoto, T. Dispersion Stability of TiO2 Particles in Aqueous Surfactant Solutions. *J. Jpn. Oil Chem. Soc.* **1993**, *42*, 501–506. [CrossRef]

68. Godinez, I.G.; Darnault, C.J.G.; Khodadoust, A.P.; Bogdan, D. Deposition and release kinetics of nano-TiO2 in saturated porous media: Effects of solution ionic strength and surfactants. *Environ. Pollut.* **2013**, *174*, 106–113. [CrossRef]

69. Zhang, C.; Lohwacharin, J.; Takizawa, S. Properties of residual titanium dioxide nanoparticles after extended periods of mixing and settling in synthetic and natural waters. *Sci. Rep.* **2017**, *7*, 9943. [CrossRef]

70. Vranic, S.; Garcia-Verdugo, I.; Darnis, C.; Sallenave, J.-M.; Boggetto, N.; Marano, F.; Boland, S.; Baeza-Squiban, A. Internalization of SiO2 nanoparticles by alveolar macrophages and lung epithelial cells and its modulation by the lung surfactant substitute Curosurf®. *Environ. Sci. Pollut. Res.* **2013**, *20*, 2761–2770. [CrossRef]

71. Chézeau, L.; Kohlstaedt, L.A.; Le Faou, A.; Cosnier, F.; Rihn, B.; Gaté, L. Proteomic analysis of bronchoalveolar lavage fluid in rat exposed to TiO2 nanostructured aerosol by inhalation. *J. Proteomics* **2019**, *207*, 103451. [CrossRef]

72. NIOSH Occupational exposure to titanium dioxide current intelligence. *Natl. Inst. Occup. Saf. Health* **2011**.

73. Gaté, L.; Disdier, C.; Cosnier, F.; Gagnaire, F.; Devoy, J.; Saba, W.; Brun, E.; Chalansonnet, M.; Mabondzo, A. Biopersistence and translocation to extrapulmonary organs of titanium dioxide nanoparticles after subacute inhalation exposure to aerosol in adult and elderly rats. *Toxicol. Lett.* **2017**, *265*, 61–69. [CrossRef] [PubMed]

74. Donaldson, E.F.; Lindesmith, L.C.; Lobue, A.D.; Baric, R.S. Norovirus pathogenesis: Mechanisms of persistence and immune evasion in human populations. *Immunol. Rev.* **2008**, *225*, 190–211. [CrossRef] [PubMed]

75. Barin, J.G.; Baldeviano, G.C.; Talor, M.V.; Wu, L.; Ong, S.; Quader, F.; Chen, P.; Zheng, D.; Caturegli, P.; Rose, N.R.; et al. Macrophages participate in IL-17-mediated inflammation. *Eur. J. Immunol.* **2012**, *42*, 726–736. [CrossRef] [PubMed]

76. Nakai, K.; He, Y.-Y.; Nishiyama, F.; Naruse, F.; Haba, R.; Kushida, Y.; Katsuki, N.; Moriue, T.; Yoneda, K.; Kubota, Y. IL-17A induces heterogeneous macrophages, and it does not alter the effects of lipopolysaccharides on macrophage activation in the skin of mice. *Sci. Rep.* **2017**, *7*, 12473. [CrossRef] [PubMed]

77. Johnson, D.E.; O'Keefe, R.A.; Grandis, J.R. Targeting the IL-6/JAK/STAT3 signalling axis in cancer. *Nat. Rev. Clin. Oncol.* **2018**, *15*, 234–248. [CrossRef]

78. Chen, L.; Wang, S.; Wang, Y.; Zhang, W.; Ma, K.; Hu, C.; Zhu, H.; Liang, S.; Liu, M.; Xu, N. IL-6 influences the polarization of macrophages and the formation and growth of colorectal tumor. *Oncotarget* **2018**, *9*. [CrossRef] [PubMed]

79. Chen, Z.; Han, Z.C. STAT3: A critical transcription activator in angiogenesis. *Med. Res. Rev.* **2008**, *28*, 185–200. [CrossRef] [PubMed]

80. Dang, C.V. c-Myc Target Genes Involved in Cell Growth, Apoptosis, and Metabolism. *Mol. Cell. Biol.* **1999**, *19*, 1–11. [CrossRef]

81. Biroccio, A.; Amodei, S.; Antonelli, A.; Benassi, B.; Zupi, G. Inhibition of c-Myc Oncoprotein Limits the Growth of Human Melanoma Cells by Inducing Cellular Crisis. *J. Biol. Chem.* **2003**, *278*, 35693–35701. [CrossRef] [PubMed]

82. Cano-Ramos, E.; Lavin, B.; Pello, O.M. Inhibition of MYC in macrophages: Tumor vs inflammation-related diseases. *OncoImmunology* **2014**, *3*, e956013. [CrossRef] [PubMed]

83. Pello, O.M.; Chèvre, R.; Laoui, D.; De Juan, A.; Lolo, F.; Andrés-Manzano, M.J.; Serrano, M.; Van Ginderachter, J.A.; Andrés, V. In vivo Inhibition of c-MYC in Myeloid Cells Impairs Tumor-Associated Macrophage Maturation and Pro-Tumoral Activities. *PLoS ONE* **2012**, *7*, e45399. [CrossRef] [PubMed]

84. Pello, O.M.; De Pizzol, M.; Mirolo, M.; Soucek, L.; Zammataro, L.; Amabile, A.; Doni, A.; Nebuloni, M.; Swigart, L.B.; Evan, G.I.; et al. Role of c-MYC in alternative activation of human macrophages and tumor-associated macrophage biology. *Blood* **2012**, *119*, 411–421. [CrossRef] [PubMed]

85. Demeterco, C.; Itkin-Ansari, P.; Tyrberg, B.; Ford, L.P.; Jarvis, R.A.; Levine, F. c-Myc Controls Proliferation *Versus* Differentiation in Human Pancreatic Endocrine Cells. *J. Clin. Endocrinol. Metab.* **2002**, *87*, 3475–3485. [CrossRef]

86. Okuyama, H.; Endo, H.; Akashika, T.; Kato, K.; Inoue, M. Downregulation of c-MYC Protein Levels Contributes to Cancer Cell Survival under Dual Deficiency of Oxygen and Glucose. *Cancer Res.* **2010**, *70*, 10213–10223. [CrossRef]

87. Zhang, P.; Li, H.; Wu, M.-L.; Chen, X.-Y.; Kong, Q.-Y.; Wang, X.-W.; Sun, Y.; Wen, S.; Liu, J. c-Myc downregulation: A critical molecular event in resveratrol-induced cell cycle arrest and apoptosis of human medulloblastoma cells. *J. Neurooncol.* **2006**, *80*, 123–131. [CrossRef] [PubMed]

88. Chuang, Y.; Hung, M.E.; Cangelose, B.K.; Leonard, J.N. Regulation of the IL-10-driven macrophage phenotype under incoherent stimuli. *Innate Immun.* **2016**, *22*, 647–657. [CrossRef] [PubMed]

89. Staitieh, B.S.; Egea, E.E.; Fan, X.; Azih, N.; Neveu, W.; Guidot, D.M. Activation of Alveolar Macrophages with Interferon-gamma Promotes Antioxidant Defenses via the Nrf2-ARE Pathway. *J. Clin. Cell. Immunol.* **2015**, *6*. [CrossRef] [PubMed]

90. Toda, M.; Mizuguchi, S.; Minamiyama, Y.; Yamamoto-Oka, H.; Aota, T.; Kubo, S.; Nishiyama, N.; Shibata, T.; Takemura, S. Pirfenidone suppresses polarization to M2 phenotype macrophages and the fibrogenic activity of rat lung fibroblasts. *J. Clin. Biochem. Nutr.* **2018**, *63*, 58–65. [CrossRef]

91. Scrima, M.; De Marco, C.; De Vita, F.; Fabiani, F.; Franco, R.; Pirozzi, G.; Rocco, G.; Malanga, D.; Viglietto, G. The Nonreceptor-Type Tyrosine Phosphatase *PTPN13* Is a Tumor Suppressor Gene in Non–Small Cell Lung Cancer. *Am. J. Pathol.* **2012**, *180*, 1202–1214. [CrossRef]

92. Takahashi, K.; Sivina, M.; Hoellenriegel, J.; Oki, Y.; Hagemeister, F.B.; Fayad, L.; Romaguera, J.E.; Fowler, N.; Fanale, M.A.; Kwak, L.W.; et al. CCL3 and *CCL4* are biomarkers for B cell receptor pathway activation and prognostic serum markers in diffuse large B cell lymphoma. *Br. J. Haematol.* **2015**, *171*, 726–735. [CrossRef] [PubMed]

93. Liu, Y.; Cai, Y.; Liu, L.; Wu, Y.; Xiong, X. Crucial biological functions of *CCL7* in cancer. *PeerJ* **2018**, *6*, e4928. [CrossRef] [PubMed]

94. Parikh, N.; Shuck, R.L.; Gagea, M.; Shen, L.; Donehower, L.A. Enhanced inflammation and attenuated tumor suppressor pathways are associated with oncogene-induced lung tumors in aged mice. *Aging Cell* **2018**, *17*, e12691. [CrossRef]

95. Cho, Y.B.; Lee, W.Y.; Choi, S.-J.; Kim, J.; Hong, H.K.; Kim, S.-H.; Choi, Y.-L.; Kim, H.C.; Yun, S.H.; Chun, H.-K.; et al. CC chemokine ligand 7 expression in liver metastasis of colorectal cancer. *Oncol. Rep.* **2012**, *28*, 689–694. [CrossRef] [PubMed]

96. Lee, Y.S.; Kim, S.-Y.; Song, S.J.; Hong, H.K.; Lee, Y.; Oh, B.Y.; Lee, W.Y.; Cho, Y.B. Crosstalk between *CCL7* and CCR3 promotes metastasis of colon cancer cells via ERK-JNK signaling pathways. *Oncotarget* **2016**, *7*. [CrossRef] [PubMed]

97. Wyler, L.; Napoli, C.U.; Ingold, B.; Sulser, T.; Heikenwälder, M.; Schraml, P.; Moch, H. Brain metastasis in renal cancer patients: Metastatic pattern, tumour-associated macrophages and chemokine/chemoreceptor expression. *Br. J. Cancer* **2014**, *110*, 686–694. [CrossRef] [PubMed]

98. Saio Tumor-associated macrophage/microglia infiltration in human gliomas is correlated with MCP-3, but not MCP-1. *Int. J. Oncol.* **2009**, *34*.

99. Pradeep, A.R.; Thorat Manojkumar, S.; Garima, G.; Raju, A. Serum levels of oncostatin M (a gp 130 cytokine): An inflammatory biomarker in periodontal disease. *Biomarkers* **2010**, *15*, 277–282. [CrossRef] [PubMed]

100. Gong, Y.; Yan, X.; Sun, X.; Chen, T.; Liu, Y.; Cao, J. Oncostatin M Is a Prognostic Biomarker and Inflammatory Mediator for Sepsis. *J. Infect. Dis.* **2020**, jiaa009. [CrossRef]

101. Oxford IBD Cohort Investigators; West, N.R.; Hegazy, A.N.; Owens, B.M.J.; Bullers, S.J.; Linggi, B.; Buonocore, S.; Coccia, M.; Görtz, D.; This, S.; et al. Oncostatin M drives intestinal inflammation and predicts response to tumor necrosis factor–neutralizing therapy in patients with inflammatory bowel disease. *Nat. Med.* **2017**, *23*, 579–589. [CrossRef]

102. Verstockt, S.; Verstockt, B.; Vermeire, S. Oncostatin M as a new diagnostic, prognostic and therapeutic target in inflammatory bowel disease (IBD). *Expert Opin. Ther. Targets* **2019**, *23*, 943–954. [CrossRef]

103. Junk, D.J.; Bryson, B.L.; Smigiel, J.M.; Parameswaran, N.; Bartel, C.A.; Jackson, M.W. Oncostatin M promotes cancer cell plasticity through cooperative STAT3-SMAD3 signaling. *Oncogene* **2017**, *36*, 4001–4013. [CrossRef] [PubMed]

104. Ayaub, E.A.; Dubey, A.; Imani, J.; Botelho, F.; Kolb, M.R.J.; Richards, C.D.; Ask, K. Overexpression of OSM and IL-6 impacts the polarization of pro-fibrotic macrophages and the development of bleomycin-induced lung fibrosis. *Sci. Rep.* **2017**, *7*, 13281. [CrossRef] [PubMed]

105. Wulczyn, F.G.; Naumann, M.; Scheidereit, C. Candidate proto-oncogene bcl-3 encodes a subunit-specific inhibitor of transcription factor NF-κB. *Nature* **1992**, *358*, 597–599. [CrossRef] [PubMed]

106. Zhang, Q.; Didonato, J.A.; Karin, M.; McKeithan, T.W. *BCL3* encodes a nuclear protein which can alter the subcellular location of NF-kappa B proteins. *Mol. Cell. Biol.* **1994**, *14*, 3915–3926. [CrossRef] [PubMed]

107. Chang, T.-P.; Vancurova, I. *Bcl3* regulates pro-survival and pro-inflammatory gene expression in cutaneous T-cell lymphoma. *Biochim. Biophys. Acta BBA Mol. Cell Res.* **2014**, *1843*, 2620–2630. [CrossRef] [PubMed]

108. Maldonado, V.; Melendez-Zajgla, J. Role of Bcl-3 in solid tumors. *Mol. Cancer* **2011**, *10*, 152. [CrossRef]

109. Guan, Y.; Yao, H.; Zheng, Z.; Qiu, G.; Sun, K. MiR-125b targets *BCL3* and suppresses ovarian cancer proliferation: miR-125b inhibits ovarian cancer cell proliferation. *Int. J. Cancer* **2011**, *128*, 2274–2283. [CrossRef]

110. Maldonado, V.; Espinosa, M.; Pruefer, F.; Patiño, N.; Ceballos-Canciono, G.; Urzua, U.; Juretic, N.; Melendez-Zajgla, J. Gene regulation by *BCL3* in a cervical cancer cell line. *Folia Biol. (Praha)* **2010**, *56*, 183–193.

111. Zhao, H.; Wang, W.; Zhao, Q.; Hu, G.; Deng, K.; Liu, Y. *BCL3* exerts an oncogenic function by regulating STAT3 in human cervical cancer. *OncoTargets Ther.* **2016**, *9*, 6619–6629. [CrossRef]

112. Wakefield, A.; Soukupova, J.; Montagne, A.; Ranger, J.; French, R.; Muller, W.J.; Clarkson, R.W.E. *Bcl3* Selectively Promotes Metastasis of ERBB2-Driven Mammary Tumors. *Cancer Res.* **2013**, *73*, 745–755. [CrossRef] [PubMed]

113. Choi, H.J.; Lee, J.M.; Kim, H.; Nam, H.J.; Shin, H.-J.R.; Kim, D.; Ko, E.; Noh, D.-Y.; Kim, K.I.; Kim, J.H.; et al. *Bcl3*-dependent stabilization of CtBP1 is crucial for the inhibition of apoptosis and tumor progression in breast cancer. *Biochem. Biophys. Res. Commun.* **2010**, *400*, 396–402. [CrossRef] [PubMed]

114. Phuyal, S.; Kasem, M.; Rubio, L.; Karlsson, H.L.; Marcos, R.; Skaug, V.; Zienolddiny, S. Effects on Human Bronchial Epithelial Cells Following Low-Dose Chronic Exposure to Nanomaterials: A 6-Month Transformation Study. *Toxicol. In Vitro* **2017**, *44*, 230–240. [CrossRef] [PubMed]

115. Sze, A.; Erickson, D.; Ren, L.; Li, D. Zeta-potential measurement using the Smoluchowski equation and the slope of the current–time relationship in electroosmotic flow. *J. Colloid Interface Sci.* **2003**, *261*, 402–410. [CrossRef]

116. Leroux, M.M.; Hocquel, R.; Bourge, K.; Joubert, O. Optimization of an innovative air-liquid interface exposure system for transcriptomic assays with semi-adherent cells. 2020; Submitted.

117. Huang, D.W.; Sherman, B.T.; Lempicki, R.A. Systematic and integrative analysis of large gene lists using DAVID bioinformatics resources. *Nat. Protoc.* **2009**, *4*, 44–57. [CrossRef]

118. Pirooznia, M.; Nagarajan, V.; Deng, Y. GeneVenn - A Web Application for Comparing Gene Lists Using Venn Diagrams. *Bioinformation* **2007**, *1*, 420–422. [CrossRef]

119. Abu-Jamous, B.; Kelly, S. Clust: Automatic Extraction of Optimal Co-Expressed Gene Clusters from Gene Expression Data. *Genome Biol.* **2018**, *19*, 172. [CrossRef]